



## Tectonics

### RESEARCH ARTICLE

10.1029/2017TC004794

#### Key Points:

- A new polyphase deformation model for the intrasalt layers in the Levant Basin is proposed
- Three distinct sets of contractional faulting affected the Messinian salt sequence
- Plio-Quaternary deformation includes strike-slip, thrust, and normal faulting

#### Supporting Information:

- Supporting Information S1

#### Correspondence to:

K. H. Kartveit,  
kyrre.kartveit@ntnu.no

#### Citation:



Kartveit, K. H., Omosanya, K. O., Johansen, S. E., Eruteya, O. E., Reshef, M., & Waldmann, N. D. (2018). Multiphase structural evolution and geodynamic implications of Messinian salt-related structures, Levant Basin, offshore Israel. *Tectonics*, 37. <https://doi.org/10.1029/2017TC004794>

Received 4 SEP 2017

Accepted 3 APR 2018

Accepted article online 19 APR 2018

## Multiphase Structural Evolution and Geodynamic Implications of Messinian Salt-Related Structures, Levant Basin, Offshore Israel

K. H. Kartveit<sup>1</sup> , K. O. Omosanya<sup>1</sup> , S. E. Johansen<sup>1</sup>, O. E. Eruteya<sup>2,3</sup>, M. Reshef<sup>4</sup>, and N. D. Waldmann<sup>3</sup>

<sup>1</sup>Department of Geoscience and Petroleum, Norwegian University of Science and Technology, Trondheim, Norway,

<sup>2</sup>Department of Earth Sciences, University of Geneva, Geneva, Switzerland, <sup>3</sup>Dr. Moses Strauss Department of Marine

Geosciences, Leon H. Charney School of Marine Sciences, University of Haifa, Haifa, Israel, <sup>4</sup>Department of Geosciences, Tel Aviv University, Tel Aviv, Israel

**Abstract** Speculations surround salt deformation in the Mediterranean Basins, both related to the deformation history and the triggers for halokinesis since the onset of the Messinian Salinity Crisis. This work presents a detailed description of the mechanisms driving internal and external deformation of a salt giant from the Levant Basin, offshore Israel. The intrasalt siliciclastic layers generate good internal reflectivity within the Messinian evaporites, allowing a thorough elucidation of the complex evolution and nature of syn-Messinian and post-Messinian structures. We have identified three distinct phases of deformation in the deep basin, based on the orientation, timing, and geometry of their related structures: The first phase is characterized by small-scaled, gravity-driven, contractional faults and folds oriented N-S that have been overprinted by a second syn-Messinian, NW-SE trending, deformation phase affecting the clastic bundles. This latter deformation phase is the cause of truncation of the intrasalt stringers on the intra-Messinian truncation surface. The third deformation phase occurred in the Pleistocene and affected all strata from the Messinian salt to the seabed. This deformational phase produced thrust, strike-slip, and normal faults, but the dominant orientation of the thrust faults and folds is NNW-SSE. Our study demonstrates that the first deformation phase was caused by regional uplift along the Levant margin during the Messinian, the second is a response to basin subsidence toward the Cyprus Arc, also syn-Messinian, and the third phase is likely related to the reorganization of the African-Eurasian plate boundary and activity along the Dead Sea Transform after the Messinian Salinity Crisis.

**Plain Language Summary** A thick body of alternating evaporites and claystones was deposited in the Mediterranean Sea during the infamous Messinian Salinity Crisis, between 5.93 and 5.33 million years ago. This event is in itself poorly understood, as both the cause(s) and the consequence(s) of this crisis is heavily disputed. In this study, we use traditional seismic interpretation as well as geometrical observations and seismic attribute analysis to understand the tectonic movements and how they have generated different fault types in the subsurface of offshore Israel during and after the deposition of the evaporite package. We present three different deformation phases and discuss their possible trigger mechanisms. The good quality of the seismic data used in the study has provided us with excellent examples of thrust, strike-slip, and normal faults in the area. These classical examples offer a clearer picture of the tectonic history of the study area, which has wider application in understanding tectonic histories of many basins worldwide.

### 1. Introduction

Salt-rich passive continental margins facilitate complex deformation of both the mobile salt and the surrounding rock mass (e.g., Allen et al., 2016; Alves et al., 2009; Cartwright et al., 2012; Cartwright & Jackson, 2008; Hudec & Jackson, 2006, 2007; Loncke et al., 2006; Netzeband et al., 2006; Rowan et al., 2012; Vendeville, 2005). The weak salt will mobilize in response to differential loading (gravity spreading) or tilting of the basin (gravity gliding), and strains within the package may be intricate and hard to reconstruct back to the original geologic setting before deformation (Bertoni & Cartwright, 2006; Cartwright et al., 2012; Gradmann et al., 2005; Hübscher et al., 2007; Netzeband et al., 2006). However, the overall trend in such a basin setting will often demonstrate a proximal thin-skinned extensional regime near the shelf and distal

contraction toward the basin due to a combination of gravity gliding and spreading (Allen et al., 2016; Cartwright & Jackson, 2008; Loncke et al., 2006; Vendeville, 2005).

In the past few decades, advances in three-dimensional (3-D) seismic interpretation and visualization have enhanced and broadened our understanding of the deformation induced by salt movement across many sedimentary basins (Cartwright & Huuse, 2005; Rank-Friend & Elders, 2004; Trudgill & Rowan, 2004). On seismic sections, the tops and bases of salt diapirs and structures are marked by distinct variation in reflectivity as a function of the drastic change in acoustic impedance across the sediment-salt interface (Brown, 2011; Jones & Davison, 2014). This is in contrast to the homogeneous nature of many salt bodies, which provide little information about their internal structures. However, when salt or evaporites are composed of “stringers” of carbonate, anhydrite, or clay, they provide good reflectors within the salt and opportunities to investigate internal salt structures and deformation (Geluk, 1998; C. A.-L. Jackson et al., 2015; C. A. Jackson et al., 2014; M. Jackson et al., 1990; Peters et al., 2003; Raith et al., 2016; Schléder et al., 2008; Strozyk et al., 2014, 2012; Talbot & Jackson, 1987; Van Gent et al., 2010).

To date, the structure and dynamics of intrasalt layers have received little attention when compared to the external shape of salt structures (Hudec & Jackson, 2006, 2007; Rowan, 1993; Vendeville & Jackson, 1992). Our current understanding of intrasalt tectonics comes from salt mines, outcrops, analogue, and numerical modeling, where complex intrasalt structures are observed on a wide range of scales (Al-Abry & Al-Siyabi, 2005; Chemia et al., 2008; Fuchs et al., 2014; Reuning et al., 2009; Schléder et al., 2008; Schultz-Ela & Walsh, 2002). Although these later techniques allow for a thorough physical description of the geometries, rheologies, and boundary conditions of intrasalt deformation, they nonetheless offer limited information on the true dimensionality and scale of intrasalt deformation, especially on a basin scale.

To understand the pattern and mechanisms of intrasalt deformation during and after salt tectonics, we have used multiple approaches, including detailed seismic interpretation, seismic attribute analyses, and structural plots, to unravel the deformational history of internal and external salt structures from the Levant Basin, Israel. The study area presents exemplary conditions in which to study intrasalt deformation and its impact on overall basin tectonics during and after salt deposition. Evaporites in the basin are young, only shallowly buried, having been precipitated quickly during the Messinian Salinity Crisis (MSC) in the Late Miocene. Most importantly, they contain laterally extensive, highly reflective layers of claystone that facilitate a thorough structural investigation of the deformation pattern(s) caused by thin-skinned tectonics (Feng et al., 2016; Feng & Reshef, 2016; Gorini et al., 2015). The reflective nature of the salt giant, as well as the absence of diapirs, also indicates that the intrasalt strains in the Levant Basin are generally low compared to other evaporite basins (Allen et al., 2016; C. A.-L. Jackson et al., 2015). Ongoing debates on the Messinian salt and its internal structures in the Eastern Mediterranean are concerned with the timing, phases, and drivers of the deformation (Allen et al., 2016; Cartwright et al., 2012; Gvirtzman et al., 2013). This has important implications for our understanding of the tectonic evolution of the region as well as the convoluted interplay of different suggested drivers and triggers of salt deformation. Our study demonstrates the complexity of intrasalt layers and their interrelationship with younger deformational phases in the study area. We have also provided classic examples of strike-slip and thrust faults associated with the Messinian salt giant in the Levant Basin that contribute to our understanding of the geodynamic evolution of the basin. The new information provided here has wider implication and application for geodynamic evolution of many similar basins worldwide.

## 2. Geological Setting of the Study Area

The study area is in the Levant Basin, offshore Israel, in the south easternmost portion of the Mediterranean Sea (Figure 1). The Levant Basin developed during multiple episodes of rifting that occurred from the Permian to Early Jurassic (Ben-Avraham, 1989; Garfunkel, 1998; Gardosh et al., 2010; Netzeband et al., 2006). During the collision of the African and European plates in the Late Cretaceous, the principal stress field of the Eastern Mediterranean and its margins translated into a compressional one, which persist until today. This compressional stress field resulted in the first stage of topographical inversion, which was associated with the formation of the Syrian arc structures (Hardy et al., 2010; Shahar, 1994). As a consequence, the Syrian Arc folds have been periodically active as of ~80 Ma, with the most recent peak in activity having been in the Early Miocene (Gardosh et al., 2006; Sagy, 2015). However, since the Late Miocene, much of the

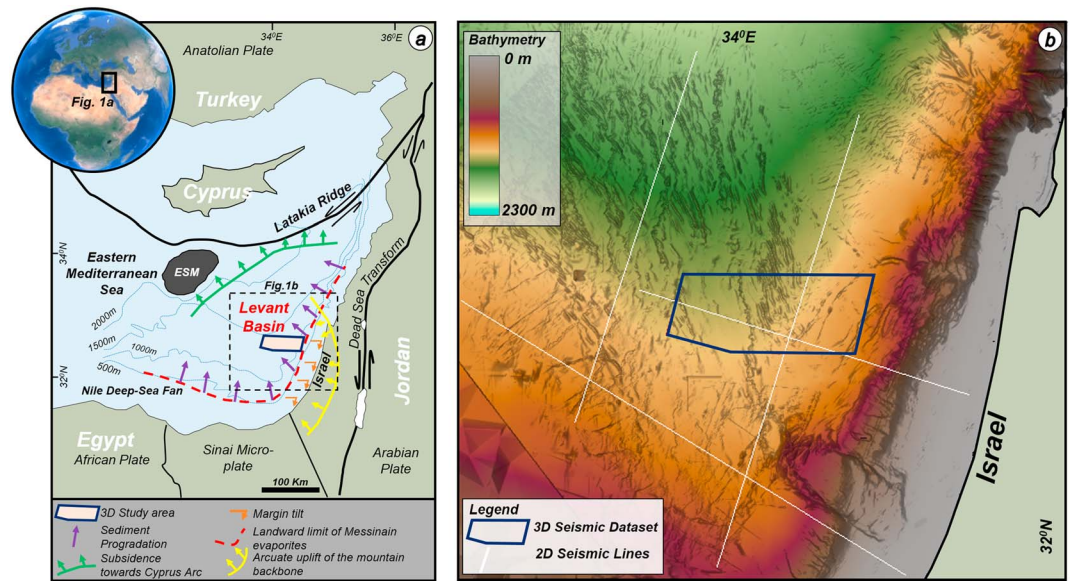


**Figure 1.** (a) Map of the Eastern Mediterranean Sea and active tectonic regimes, regional fault systems and current sediment progradation. (b) Bathymetric map of the Levant basin showing the location of the regional 2-D seismic lines and the 3-D seismic data set utilized in this work.

movement related to the compressional stress has moved inland from the offshore basin to the onshore Dead Sea Transform (Figure 1a).

Uplift during the Oligocene resulted in significant erosion of the Levant margin and the formation of wide and deep canyons (Druckman et al., 1995). These canyons were periodically excavated in several episodes during the Oligocene and Miocene, and in combination with initial supply from North African river systems, led to the accumulation of a thick sedimentary blanket in the basin, which is composed primarily of pelagic marls (Gardosh et al., 2008). At the end of the Miocene (Messinian; 5.93–5.33 Ma), a multilayered evaporitic sequence called the Messinian Evaporites was deposited across the circum-Mediterranean basins in response

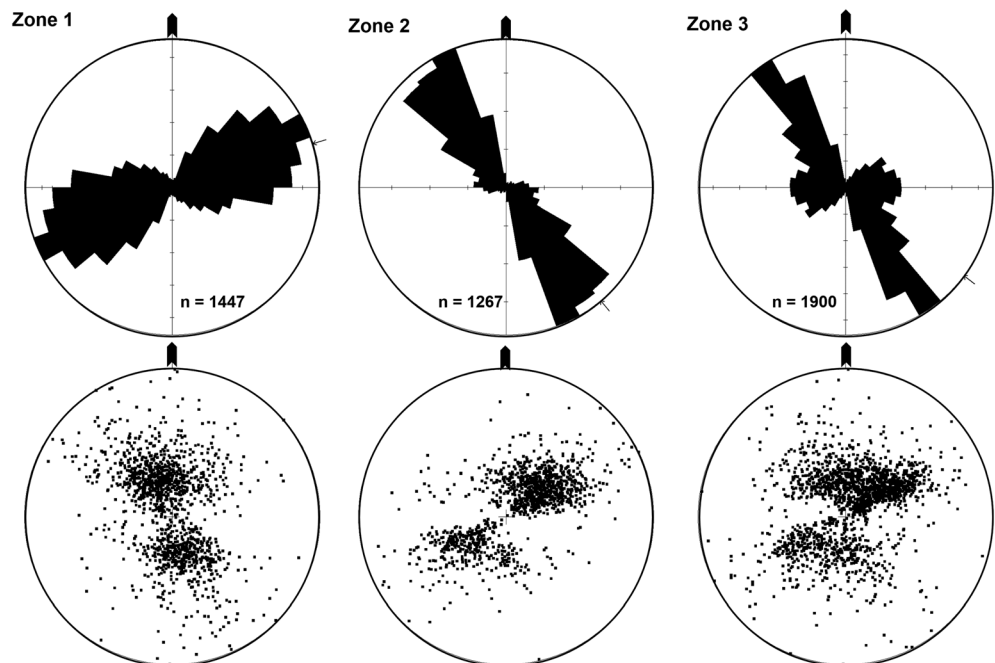


**Figure 2.** Rose diagrams (top row) and dip plots (bottom row) of the extracted faults in the three structural domains.



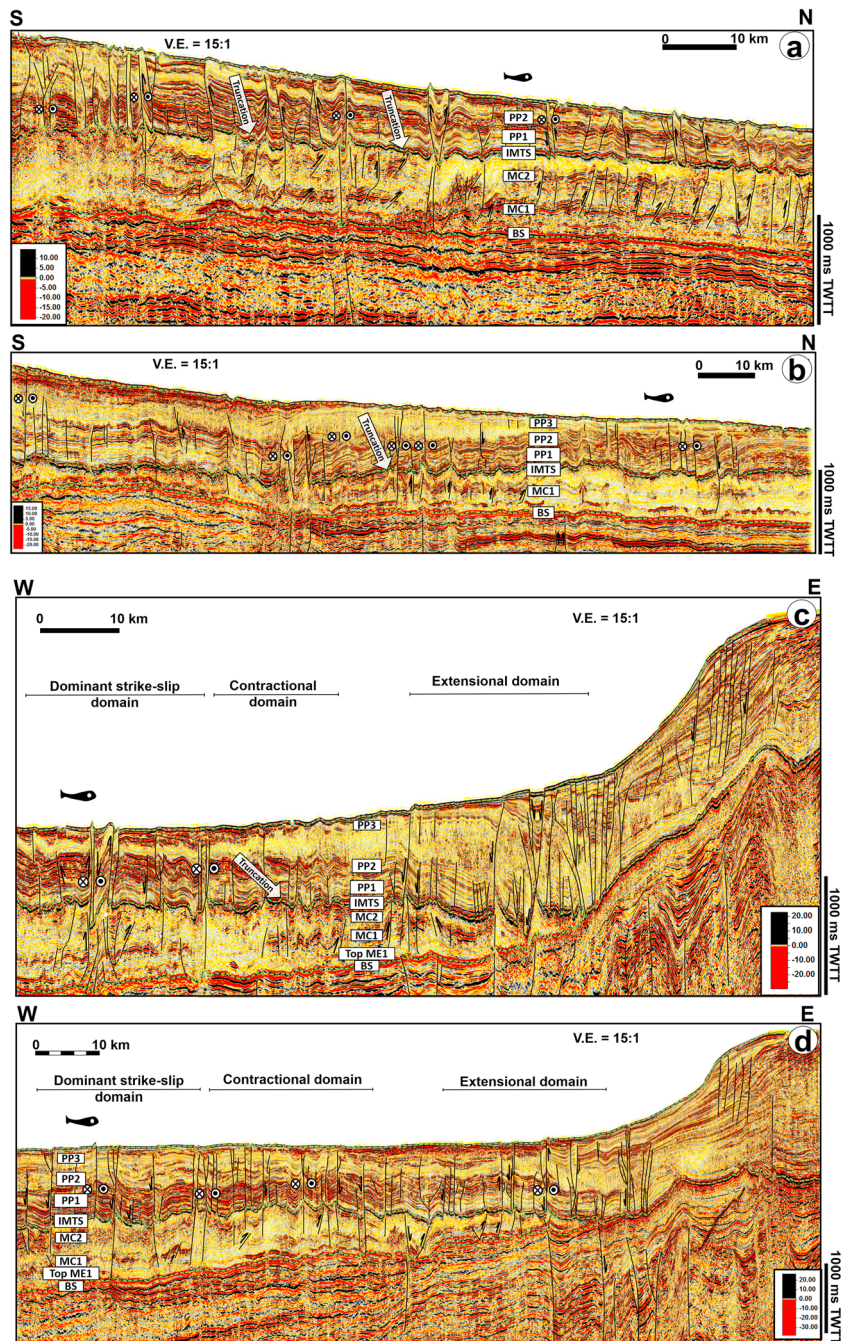


**Figure 3.** Interpretation of main faults and key horizons on four regional 2-D lines in vicinity of the 3-D data set. Panels (a) and (b) are oriented N-S, while panels (c) and (d) have a E-W configuration that illuminates the three dominant stress domains in the area. The sections show that both the seabed and the Messinian salt have a general dip toward the NE. Exact location of the lines is seen on Figure 1b. Uninterpreted 2-D lines can be found in the supporting information.

to the MSC (Hsü et al., 1973; Ryan, 1978; Roveri et al., 2014). In the Levant Basin, the Messinian Evaporites are up to 2 km thick, consist of alternating halite and clastics and anhydrite (Bertoni & Cartwright, 2006; Feng et al., 2016; Gvirtzman et al., 2017), and can be divided into seven intervals (Gvirtzman et al., 2017). At the end of the salinity crisis, a continuous supply of sediments during the Plio-Quaternary resulted in accumulation of nearly a kilometer of fine-grained sediments in the Levant Basin and over 1.5 km of sandy and silty sediments on the Levant margin (Gardosh et al., 2008), which are currently prograding basinward (Hübscher et al., 2016; Lazar et al., 2016).



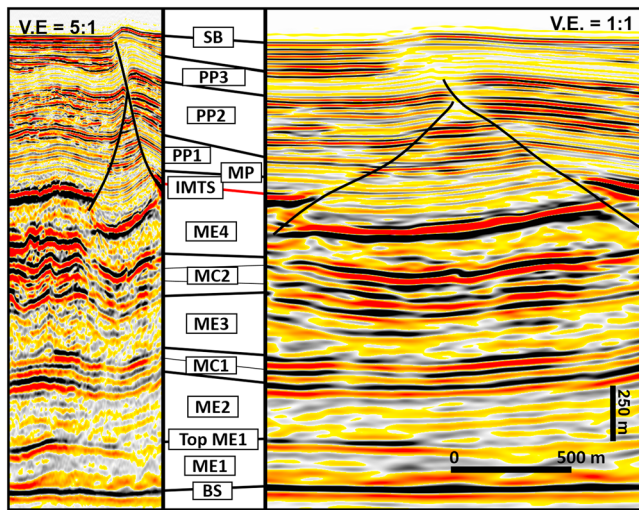


**Figure 4.** Seismic stratigraphic framework used in this study, based on the work by Feng et al. (2016) and Gvirtzman et al. (2017). Nomenclature is taken from these studies, with the exception of the MP reflection, which signifies the Messinian-Pliocene boundary, and the PP1-PP3 seismic packages in the Plio-Quaternary overburden.

The Plio-Quaternary unit along the margin and basin have been deformed as a consequence of gravitational tectonics, basement tilting, and likewise successive episodes of submarine mass wasting (Cartwright & Jackson, 2008; Frey Martinez et al., 2005; Eruteya et al., 2016; Gvirtzman et al., 2015; Katz et al., 2015; Tibor et al., 1992). Onshore uplift related to the Dead Sea Transform and its secondary fault system, the Carmel fault, appears to have resulted in early deformation within the salt sequence during its deposition (Gvirtzman et al., 2013); however, this is strongly disputed by Allen et al. (2016). The principal deformation of the salt layers occurred during the Plio-Quaternary with the loading of the Nilotic sediments atop the southeastern margin of the Eastern Mediterranean (Allen et al., 2016), leading to folding and diapirism.

### 3. Data and Approach

Our study is based on seismic interpretation of a high-resolution, high-quality, prestack zero-phase, depth-migrated 3-D seismic reflection survey covering approximately 1,600 km<sup>2</sup> (Figure 1). The seismic cube has crossline (N-S) and inline (E-W) spacing of 25 m and 12.5 m, respectively, and the vertical sampling rate of the cube is 3 m. Final migration yielded a depth-migrated volume having a vertical and horizontal resolution of ~6 m.

In addition to this, four regional 2-D lines have been interpreted to address the broad basin-wide structural domains and extent of intrasalt deformation. These lines are displayed in the time domain with a sampling rate of 2 ms. All of the seismic data in this study are displayed with the normal convention adopted by the Society of Exploration Geophysicists (normal SEG polarity), whereby a downward increase or decrease in acoustic impedance correspond to a positive (red) or negative (black) reflection, respectively.

Seismic interpretation of the principal horizons was done at intervals of 125 m and 250 m on the inlines and crosslines, respectively, to constrain the general geology of the study area. These horizons include the seabed

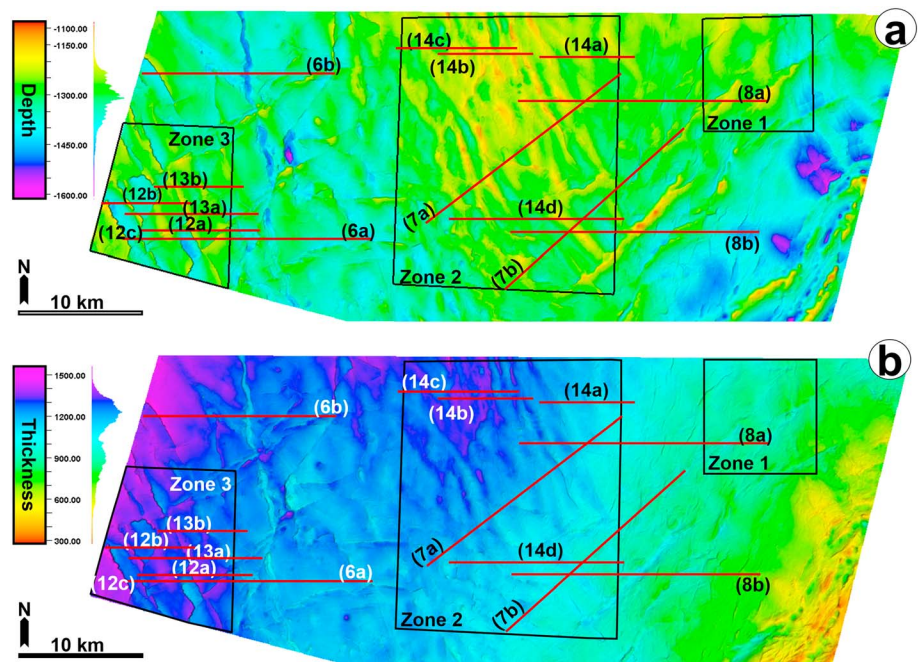


**Figure 5.** (a) Interpreted intra-Messinian truncation surface surface and (b) thickness map of the entire Messinian package. Three distinct structural domains have been defined (Zones 1–3), and selected seismic sections are shown on the maps.

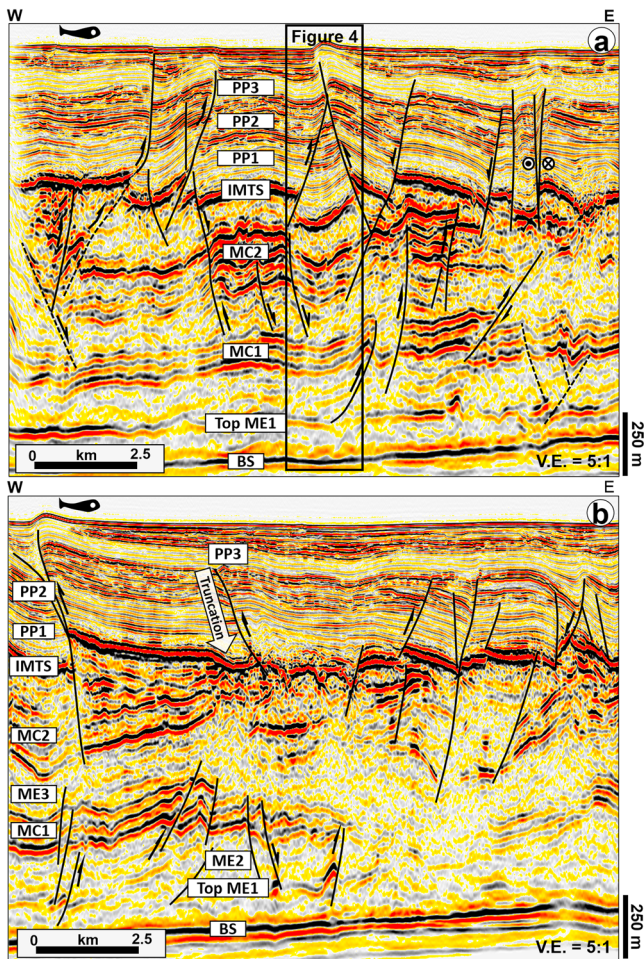


**Figure 6.** E-W oriented seismic sections through (a) Zone 3 and (b) the north-western part of the study area showing examples of different thrust faults and key horizons.

reflection, intra-Messinian truncation surface (IMTS), Top MC2, Base MC2, Top MC1, Base MC1, Top ME1, and the base salt (BS; Feng et al., 2016; Gvirtzman et al., 2017). The seabed and IMTS were used to automatically extract structural information at different depths. This exercise entails the extraction of surfaces at certain depths, for example, 50 m, 100 m, and 250 m below and above either of the horizons. In addition to seismic interpretation, multiple seismic attribute analysis was conducted to elucidate the internal structures of the intrasalt layers. The seismic attributes used in this work are structural smoothing, variance, Gaussian curvature, and dip angle. The structural analysis consists of the use of ant tracking for automatic fault extraction, along with rose diagrams and equal area projections (Figure 2). A key structural technique is the use of curvature attributes to characterize the top salt, MC1 and MC2 folds.

The structural smoothing attribute was applied to the seismic data. This attribute smooths the input data guided by local structures, thereby increasing the signal-to-noise ratio and improving the continuity of seismic reflectors. This will sharpen the boundaries of the reflectors, making the data suitable for structural interpretation (Fang et al., 2017). The variance seismic attribute was used to identify the faults because it is a direct measurement of the dissimilarity of seismic traces. Hence, variance maps convert a volume of continuity into a volume of discontinuity, highlighting structural and stratigraphic boundaries (Brown, 2011). Faults represent trace-to-trace variability and are mapped with high variance coefficients. Furthermore, an ant tracking algorithm was utilized in order to track and sharpen faults. The algorithm distributes a population of digital ants that are coded to follow discontinuities in the seismic volume. The swarm intelligence will then promote the computer agents to follow identified discontinuities and avoid known noise sources (Abul Khair et al., 2012; Cox & Seitz, 2007). Faults are automatically extracted once the ant tracking cube is generated. In addition to the automatic fault extraction, interpretation of complicated fault types such as strike-slip faults in the study area was further validated using struc-

tural maps and geomorphological features such as channels. This is most important to ascertain their true sense of lateral movement.

To characterize folds associated with thrust faults, the curvature and dip angle seismic attribute was used. The curvature is simply a measure of how tightly folded a surface is at a particular point (Lisle, 1994). In 3-D, folds are characterized by minimum curvature, that is, the wider radius and maximum curvature, the smallest radius of the fold. The more tightly folded a surface is, the larger its curvature. The curvature attribute is a fantastic tool for mapping the hinge line of folds. The other types of curvature used are mean and Gaussian curvatures. Local dip angles were extracted using the dip angle attribute, which calculates the dip of a reflector by comparing each trace with the surrounding traces.

## 4. Observations and Interpretations

### 4.1. Interpreted Seismic Units

The seismic-stratigraphic framework used here (Figures 3 and 4) is similar to that used by Feng et al. (2016) and Gvirtzman et al. (2017). We have adopted the nomenclature and lithological interpretations proposed by Feng et al. (2016) but acknowledge the interpretation of the regional unconformity as an intra-Messinian truncation surface and the presence of a late-Messinian sediment package overlying the truncation surface (Gvirtzman et al., 2017). The IMTS is a strong, faulted, high-amplitude reflection, which regionally dips in the north-northwestern direction (Allen et al., 2016; Netzeband et al., 2006), although it appears horizontal



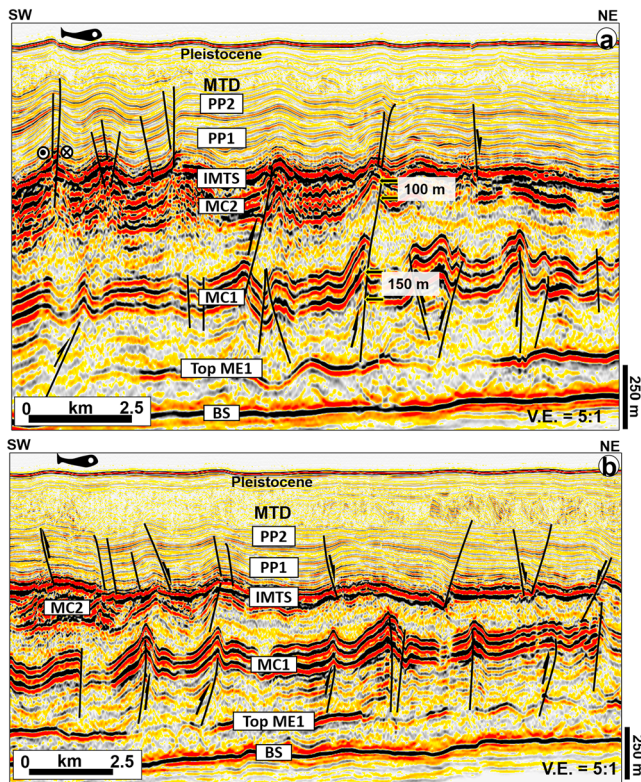


**Figure 7.** (a and b) NE-SW oriented seismic sections through the contractional domain (Zone 2) showing considerable thrusting in the Messinian salt and folding in the Pliocene succession. Note the decrease in throw on the dominant intrasalt thrust fault in the MC2 package compared to the MC1.

in our 3-D data (Figure 5a). At the base of the salt unit is the BS horizon which is a relatively strong, flat, and continuous reflection. The high-amplitude reflector overlying the BS is generally discontinuous and fades out on the eastern parts of the survey. Where it is observable, it is subparallel to the BS. This is interpreted as the Top Messinian Evaporite 1 (see, e.g., Figures 4, 6a, 7, and 8; Feng et al., 2016). In between the Top ME1 and the BS, only nearly transparent and low-amplitude reflections can be seen, except in the northeastern part of the seismic cube where a high-amplitude, chaotic package is found overlying the BS. The units overlying the Top ME1, ME2, are also characterized by transparent to low-amplitude reflections (Figures 6a and 7).

On top of the transparent ME2 is a package of three to four high-amplitude, strongly deformed reflections (Figures 3 and 7). This package is the first Messinian clastic bundle, MC1, and is separated from the second Messinian clastic bundle, MC2, by a zone of low amplitude to transparent reflections, ME3 (Figure 7). The lithological characters of the clastic bundles have been heavily debated, but cross plots of seismic velocities, densities, and neutron porosities have shown that they mainly consists of claystones (Feng et al., 2016). The second Messinian clastic bundle is restricted to the western part of the study area and is inclined against the IMTS reflections indicating erosional truncation (Figures 8b and 14c). Both clastic bundles have gentle dips to the west at an average angle of approximately 1° (Figures 3 and 9). The unit between the MC2 and the IMTS, ME4, is also low amplitude to transparent and is restricted to the western part of the study area. Overall, all the units are generally truncated by the IMTS with the amount of truncation gradually increasing eastward (Figures 3c and 3d). East of the 3-D seismic cube, the IMTS and BS amalgamate, giving the

Messinian Evaporites a general wedge-shaped geometry that thickens toward the NW and pinches out along the eastern margin (Figures 3c and 3d).

Lithologically, the four low-amplitude, chaotic packages described here are composed of pure halite, whereas MC1 and MC2 are composed of clastic sequences comprising bundles of thin clay layers (averaging 2 m within MC1 and 1.5 m in MC2) interbedded in the halite background (Feng et al., 2016; Gvirtzman et al., 2013). A thin unit consisting of alternating anhydrite, sand, and clay layers with a cumulative thickness of ~100 m is found directly above the IMTS (Gvirtzman et al., 2017). The top of this unit is characterized by a downward increase in acoustic impedance and represents the Miocene-Pliocene boundary. The Plio-Quaternary units above the IMTS consists of Nile-derived sediments, as well as clay-rich marls, sandstones, and claystones and slump complexes sourced from the Levantine continental margin (Ben-Gai et al., 2005; Eruteya et al., 2015; Frey Martinez et al., 2005; Gvirtzman et al., 2015; Tibor & Ben-Avraham, 2005).

#### 4.2. Structural Domains

The style of structures associated with the Messinian salt units and their intrasalt layers (MC1 and MC2) is best described using the IMTS and the top MC1 and MC2 structural maps (Figures 5 and 9). The IMTS structural map as well as the regional 2-D seismic sections revealed three distinct structural domains, which include an easternmost domain where normal faults dominate (Zone 1), an intermediate domain characterized by compressional structures or simply thrust faults (Zone 2), and a western domain dominated by strike-slip and thrust faults (Zone 3; Figures 4 and 5).

Zone 1 is characterized by large-scale normal faults that interact with thrust and strike-slip faults (Figures 5, 8, and 10f). The general strike of faults in Zone 1 is ENE-WSW with dips dominantly to the WNW (Figures 3 and 5a). Horst, graben, and rotational faulting systems can be seen on the western edge of the zone (Figure 8). The majority of the fault planes are planar to being rotated (Figures 3c and 8). The other faults



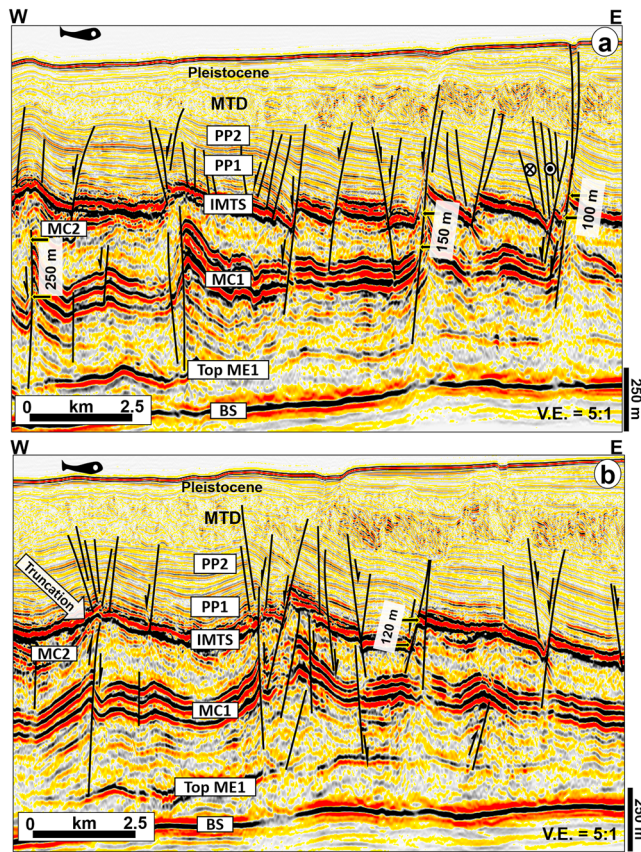


**Figure 8.** (a and b) E-W oriented seismic sections in the eastern part of the study area showing extensive normal faulting in the extensional domain (Zone 1). Throws of some of the main faults are indicated in the green boxes.

and structures in Zone 1 include strike-slip faults extending from Top ME1 into the Plio-Quaternary sequence, Plio-Quaternary rollover anticline structures, and intrasalt thrust faults and related folds (Figures 4c and 8).

The general orientation/structures in Zone 2 include NNW-SSE and NW-SE thrust faults (Figures 3, 5, and 7). Minor strike-slip faults in Zone 2 usually interact with the thrust faults (Figure 7a). The strike-slip faults can be very hard to recognize on seismic sections, but offset of channels, faults, and folds in the post-Messinian succession has been identified on horizon slices and attribute maps. The dip angle for faults in Zone 2 ranges from  $<10^\circ$  to almost  $90^\circ$  in the NE and SW directions (Figure 2). Conversely, Zone 3 is dominated by NNW-SSE thrust faults and folds (Figures 3 and 6a). Dip angle for the thrust faults ranges from  $10^\circ$  to  $30^\circ$  (Figure 2). Thrust faults in Zone 3 are usually intersected by conjugate strike-slip faults (Figure 11). On seismic sections, the strike-slip faults are marked as vertical or near-vertical faults that offset the MC1, MC2, IMTS, and the overlying post-Messinian strata (Figure 12c) and usually detach into any of the ME4, ME3, or ME1 evaporites (Figures 4a and 4b, and 13).

### 4.3. Fault Types Affecting the Syn-Messinian and Post-Messinian Successions

We observe steeply dipping sinistral strike-slip faults that strike in the NE-SW direction (Figure 11). These faults are seen both internally in the salt and in the suprasalt sequences (Figures 12c and 13b) and have lateral displacements of up to approximately 900 m in the eastern part of the study area (Figure 11). Three classes of strike-slip fault types that occur in the study area are (a) Type I strike-slip faults characterized by pop-up structures associated with contractional bends. The associated flower structures are seen largely within the post-Messinian succession as well as on smaller scale faults in MC1 (Figures 12 and 13). (b) Type II

strike-slip faults form negative flower structures on seismic sections and are common in the Messinian and the Plio-Quaternary strata (Figure 13b). The last group of strike-slip faults is (c) Type III, which includes planar, isolated, and vertical faults, mainly localized within the Plio-Quaternary succession and occasionally piercing deep into the ME1 (Figures 4b and 13b).

Thrust faults include those offsetting the Messinian package and Plio-Quaternary succession. The intrasalt thrust faults are predominantly striking NNW-SSE, with varying angles of dip (Figures 6 and 10a and 10b), offsetting MC1 and MC2 (Figures 7 and 9). Within MC1, the thrust faults change strike from almost NNW-SSE in the northernmost part of Zone 2 to NW-SE in the south (Figure 9). Other thrust faults deforming MC1 include small-scale, N-S oriented thrust faults in Zone 2 (Figures 10a and 14). The dominant NNW-SSE trending thrusts normally have a larger displacement than the aforementioned faults and causes the MC2 to fold with vergence generally to the ENE (Figures 5 and 7), even though back thrusts with opposite vergence trend are often seen. Displacement on the NNW-SSE thrusts can reach up to 150 m within the MC1 and 100 m in the MC2 (Figure 7a), whereas displacement of the N-S faults rarely exceeds 100 m (Figures 7a and 10a). The Top ME1 reflector seems to act as a lower decollement for the intrasalt thrusts. The majority of the thrust faults that offset IMTS to ME1 also offset the overlying Plio-Quaternary succession (Figure 7a).

The suprasalt thrust faults have a similar trend as the dominant intrasalt thrust faults (Figure 9) but are much more prominent in terms of throw and heave. Throws of the suprasalt thrust faults can reach up to 240 m (e.g., Figure 12a). These faults typically detach on the closest transparent facies, for example, ME4 beneath the IMTS reflector. Near their upper tip positions, onlapping reflections of Late Pleistocene age are seen, suggesting the timing of fault formation (Figures 12a and 12b). A common expression of active thrusting attributed to these faults are ridges seen on the seabed map signifying that the thrust faults are formed post-Messinian and is still ongoing (Figures 1 and 12c). The post-Messinian thrust faults at the Pliocene

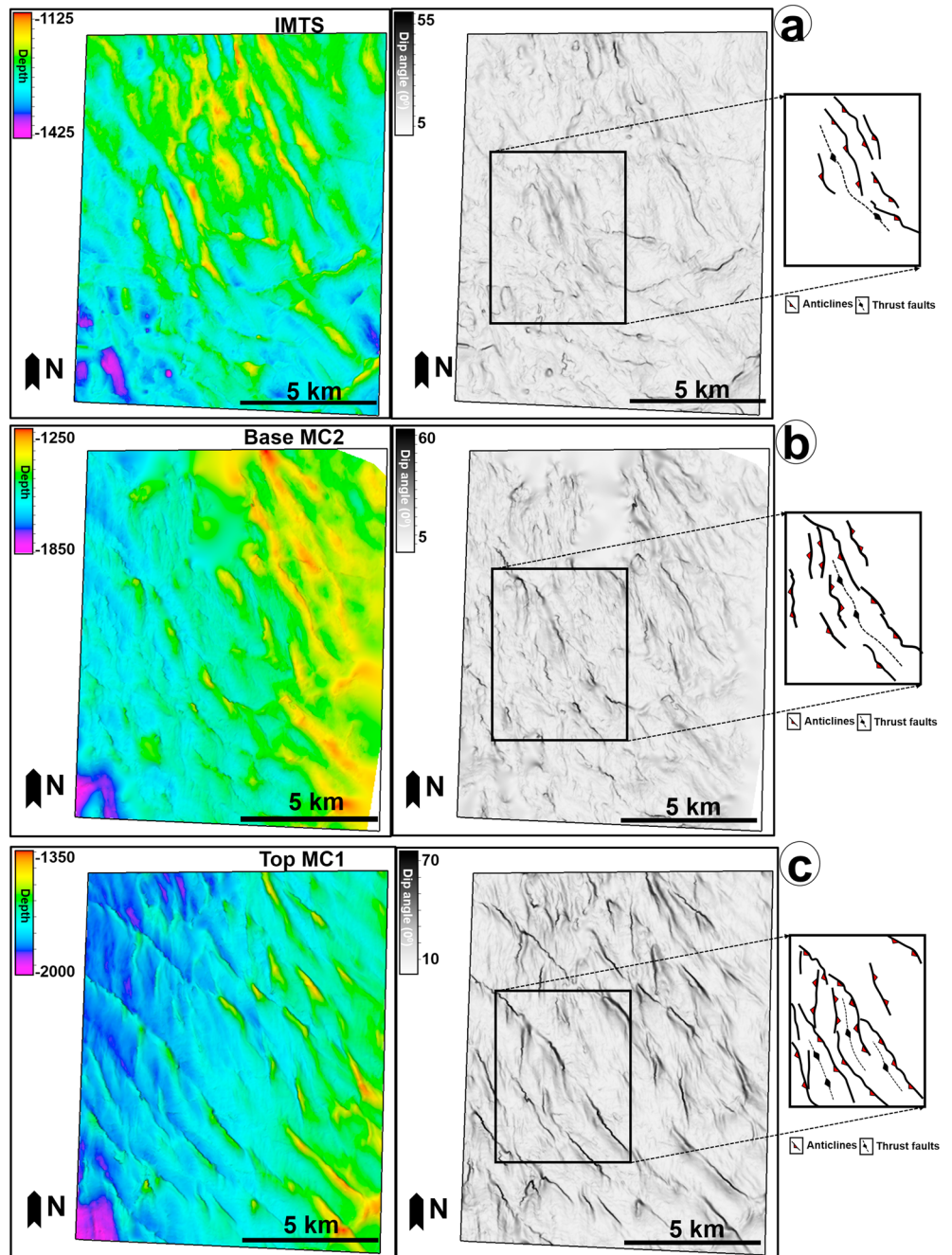


**Figure 9.** Structural maps (left column) and dip illumination maps (right column) discriminating deformation trends of (a) the IMTS surface, (b) the base of MC2, and (c) the top MC1 reflectors within Zone 2. Note the decrease in deformation on the shallower reflections as well as the clockwise rotation of the deformation structures.

interval show evidence of fault propagation with trishear geometries (see Allmendinger, 1998; Erslev, 1991). Additionally, the thrust faults can form a train composed of a leading thrust and trailing thrusts, with the main decollement being the IMTS surface, but with some of the larger thrusts rooted in the Messinian salt sequence (Figures 10c and 12a). Thrust faults with back thrusts are also seen at this level (Figures 6a and 10d). When two thrust faults have opposing directions of vergence, they can develop triangle zones, with the thrust faults detaching near the IMTS horizon (e.g., Figure 12b). Some of these triangle zones can sometimes be offset by positive flower structures (Figure 12c).



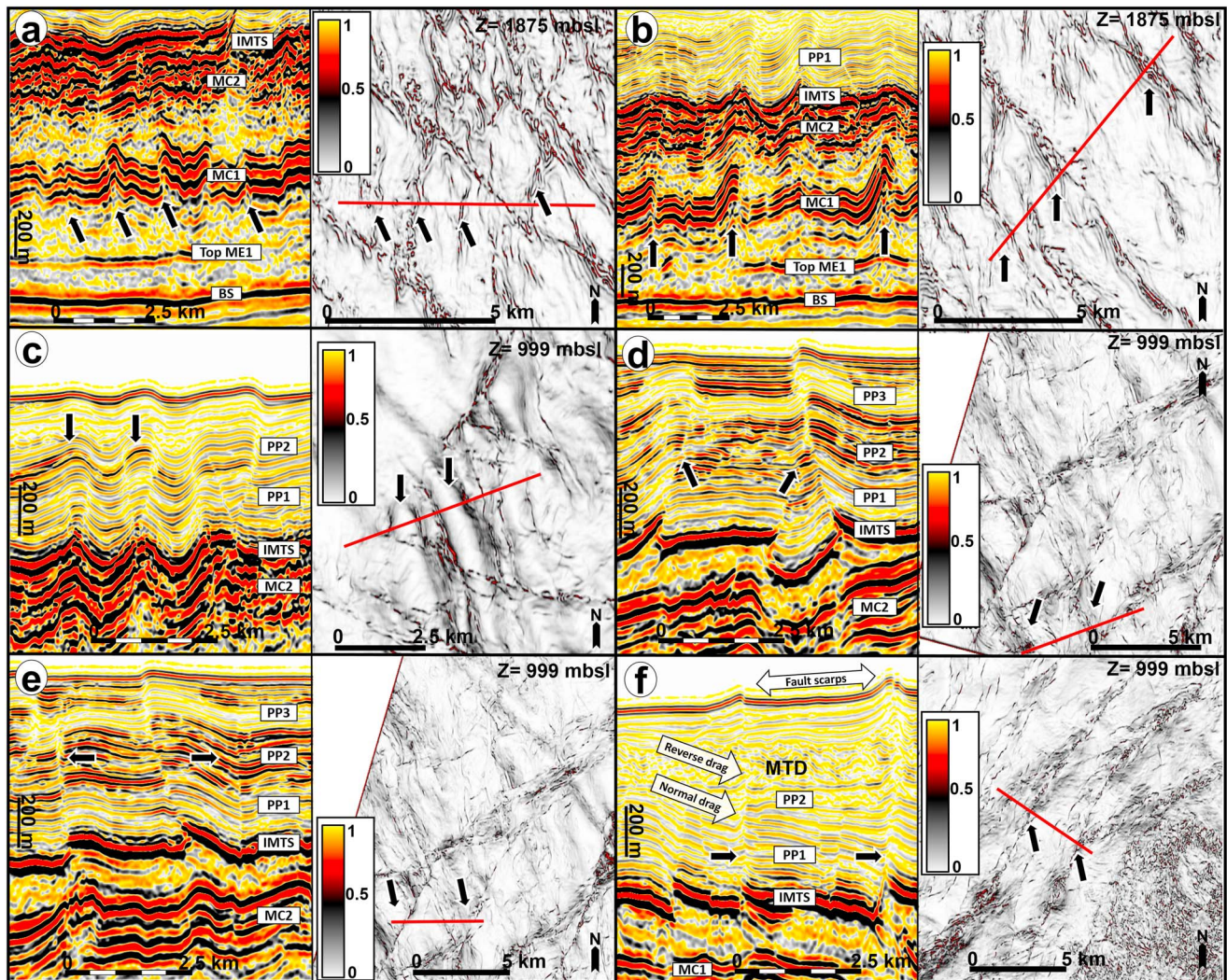


**Figure 10.** Examples of the different thrust types seen in the study area on seismic sections (left) and variance time slices (right): (a) intrasalt N-S trending thrust faulting, (b) intrasalt NNW-SSE trending thrust faulting, (c) contractional folding in the Messinian salt and the Plio-Quaternary succession, (d) major thrust faulting of post-Messinian sediments, (e) strike-slip faulting, and (f) master normal faults. The color bars signify the coefficient of variance. Faults are marked as moderate to high variance coefficients as compared to the surrounding strata of low variance coefficients.

The last group of faults in the study area consists of normal faults, which generally strike in the NE-SW direction, but ranges from an almost N-S trend in the northeastern part of the survey to an ENE-WSW orientation in the southeast (Figures 5a and 10f). Normal faults in the study area are mainly large-scaled growth faults intersecting the MC1 and the IMTS and scattered extensional faults which are often truncated at the base of the overlying mass transport deposit (MTD; Figures 4c, 8a, and 10f). The large-scale normal faults strike parallel to the shelf edge in Zone 1 extending from the base salt and into the Pleistocene layers above the MTD, sometimes displacing the seabed (Figures 4c and 4d, and 8a). Furthermore, suprasalt normal faults offsetting the overlying MTD are common in Zone 1 but are also seen elsewhere in the study area. Normal faults have up to 1.5 km of displacement at the MC1 and up to 1 km at the IMTS level (e.g., Figure 5a). The dominant, large-scale, normal faults are generally listric faults, while the more scattered smaller-scaled normal faults are generally more planar.

#### 4.4. Other Intrasalt Structures

Apart from intrasalt thrust faults discussed above, MC1 and MC2 are also characterized by other compressional structures such as folds, ramp complexes, and pop-up structures (Figures 10a and 10b and 14). The



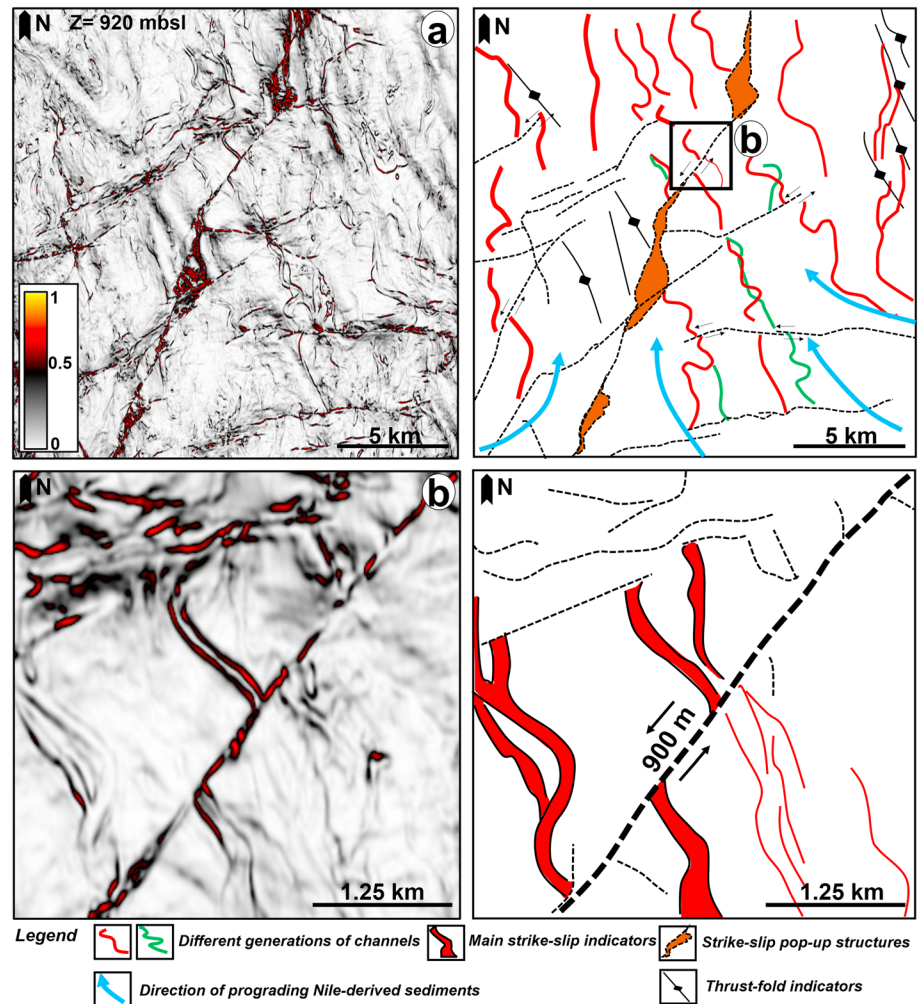


**Figure 11.** (a) Variance time slice through the post-Messinian succession in Zone 3 showing substantial strike-slip faulting as well as NNW-SSE oriented contractional structures and (b) close up of one of the major strike-slip faults. Main channel systems, proposed sediment progradation and major push-up ridges are indicated in the interpretations.

ramp complexes are present in the MC1 strata, whereas the thrust faults and folds are present in both MC1 and MC2, the pop-up structures are visible internally in MC1 in Zones 2 and 3 (Figures 13b and 14a). The principal thrust faults strike NW-SE and N-S (Figures 13 and 14). Where the two sets of thrust faults overlap, they are superimposed and this causes locally large offsets of the MC1 sequence, reaching a maximum throw of approximately 300 m (Figure 10b). The N-S trending faulting seems to be quite scattered, but most prominent in Zone 2, while the NW-SE to NNW-SSE striking thrust faults are obviously present everywhere in the study area (Figures 5a and 9). Additionally, the MC1 package is laterally continuous perpendicular to the fault trend, except in a 6 km wide transparent band that trends NNW-SSE between Zone 2 and 3 (Figures 4c and 4d, 6b, 9a, and 9b). This band represents areas of poor seismic imaging likely associated with subsurface fluid plumbing (e.g., Claudia Bertoni and Cartwright, 2015) or, alternatively, areas of homogeneous rock and/or high strains (C. A.-L. Jackson et al., 2015). This is also the case for all intrasalt reflections, making it difficult to trace structural trends from the eastern part of the study area to the west. The MC2 package is less influenced by intrasalt faulting than MC1 but is subject to folding above the most prominent NNW-SSE striking master thrust faults. However, it is important to note that not all intrasalt thrusts deform the MC2 strata. In contrast, the MC2 sequence is often subject to faulting related to the major strike-slip and thrust faulting seen in the Plio-Quaternary succession that is rooted in the Messinian salt, especially where the ME4 package is absent between MC2 and IMTS (Figures 6 and 13). The entire MC2 sequence is only imaged in the western part of the study area, where it

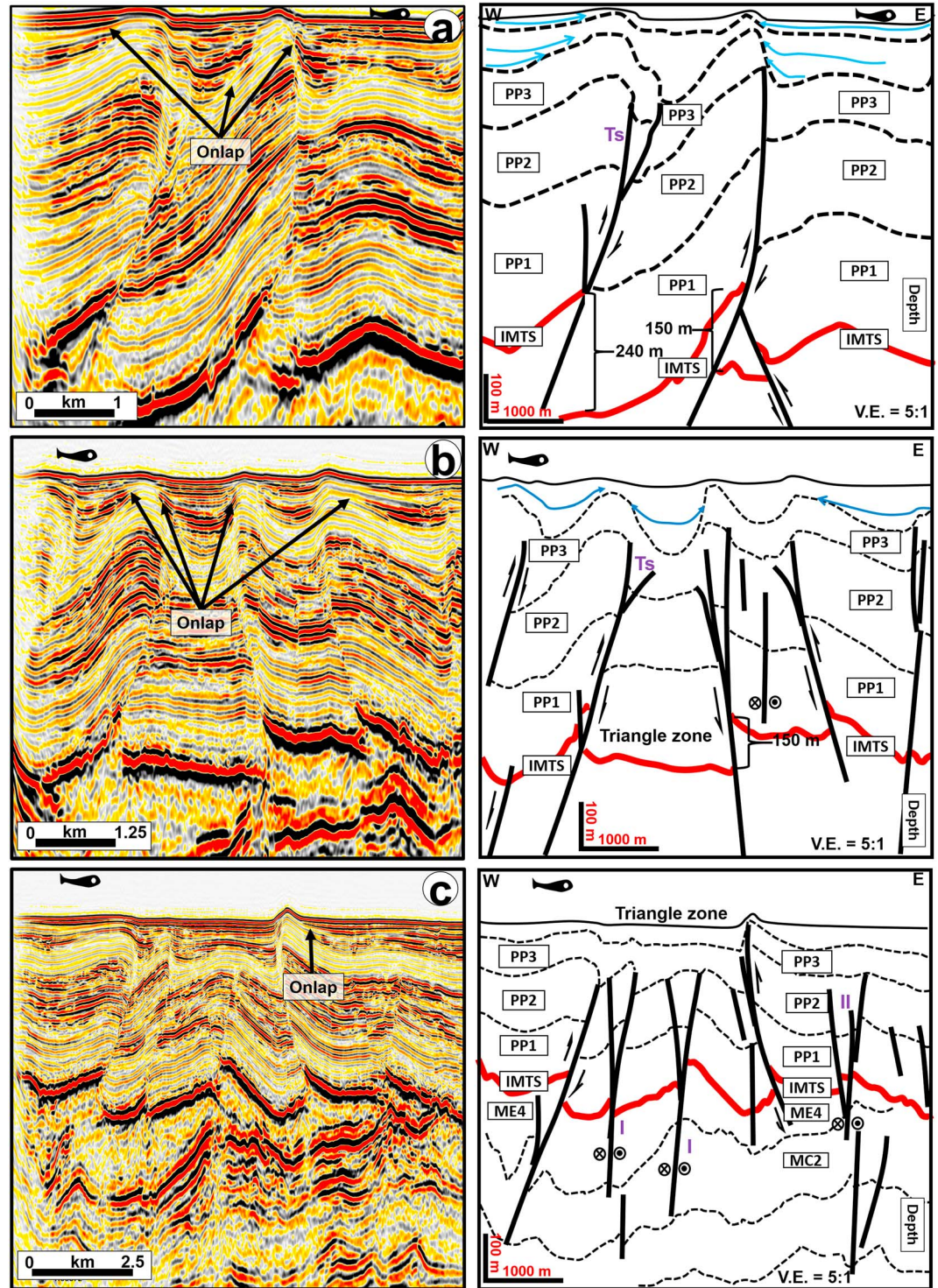


**Figure 12.** (a–c) Examples of different thrust-and strike-slip faults in Zone 3. Throws of some of the major faults are indicated on the interpretations, as well as onlapping relationships and key horizons. Note the trishear geometry of some of the master thrust faults and the presence of triangle zones where the thrusts have opposite dips.



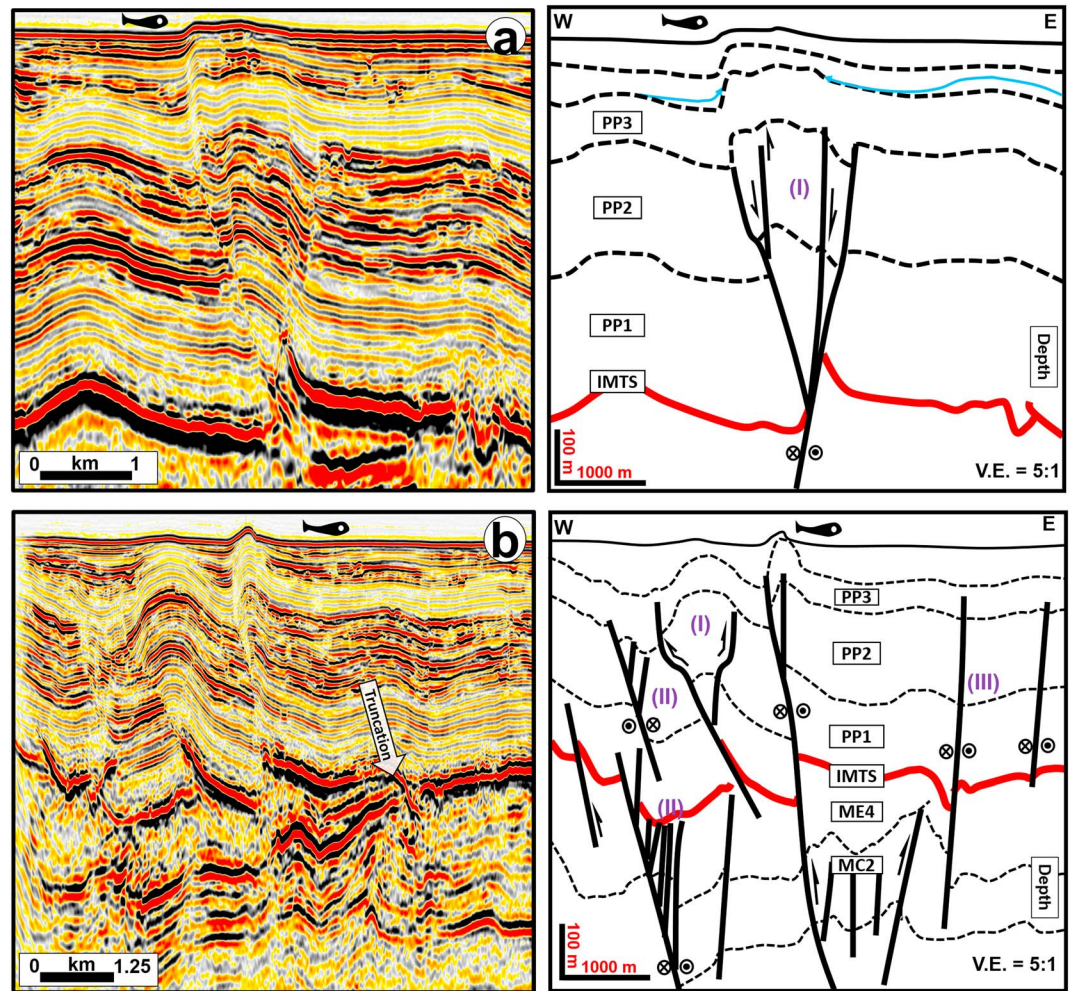


**Figure 13.** (a and b) Different types of strike-slip faults seen in the strike-slip domain (Zone 3). Note the onlapping relationship of the Pleistocene reflections below the seabed.

is overlain by the transparent ME4 sequence (Figures 6 and 10d and 10e). This is also where the package is most continuous and undeformed. It is very difficult to address strike-slip faulting in the salt package due to lack of morphological features within MC1 and MC2, unless they are vertically traceable throughout the Plio-Quaternary overburden and into the salt. Internal patterns and terminations of reflectors can also be deceptive, and care should be exercised especially when interpreting seismic data in areas with contractional structures (Johansen, 2013; Johansen et al., 1994). For this reason, intrasalt strike-slip faulting in the Messinian sequence will not be discussed in detail in this article.

## 5. Discussion

### 5.1. Mechanisms and Styles of Faulting and Folding in the Study Area

Strike-slip faults in the study area are generally vertical NE-SW oriented sinistral to NW-SE oriented dextral faults forming conjugate sets (Figure 11). However, the strike-slip faults have not been thoroughly mapped in this work. We acknowledge that strike-slip faults often strike approximately 30° to the horizontal compression direction, which fits the observed cross-cutting relationship between the thrust faults and the strike-slip faults in our study area. The strike-slip faults vary in orientation, and the Type II strike-slip fault zones in particular seem to have a more ENE-WSW orientation to the oppositely dipping faults. Where major thrust faults interact with the strike-slip faults, compressional zones develop with many well-developed positive flower structures that are bounded by convex-up faults, that is, Type I thrust faults (see McClay and



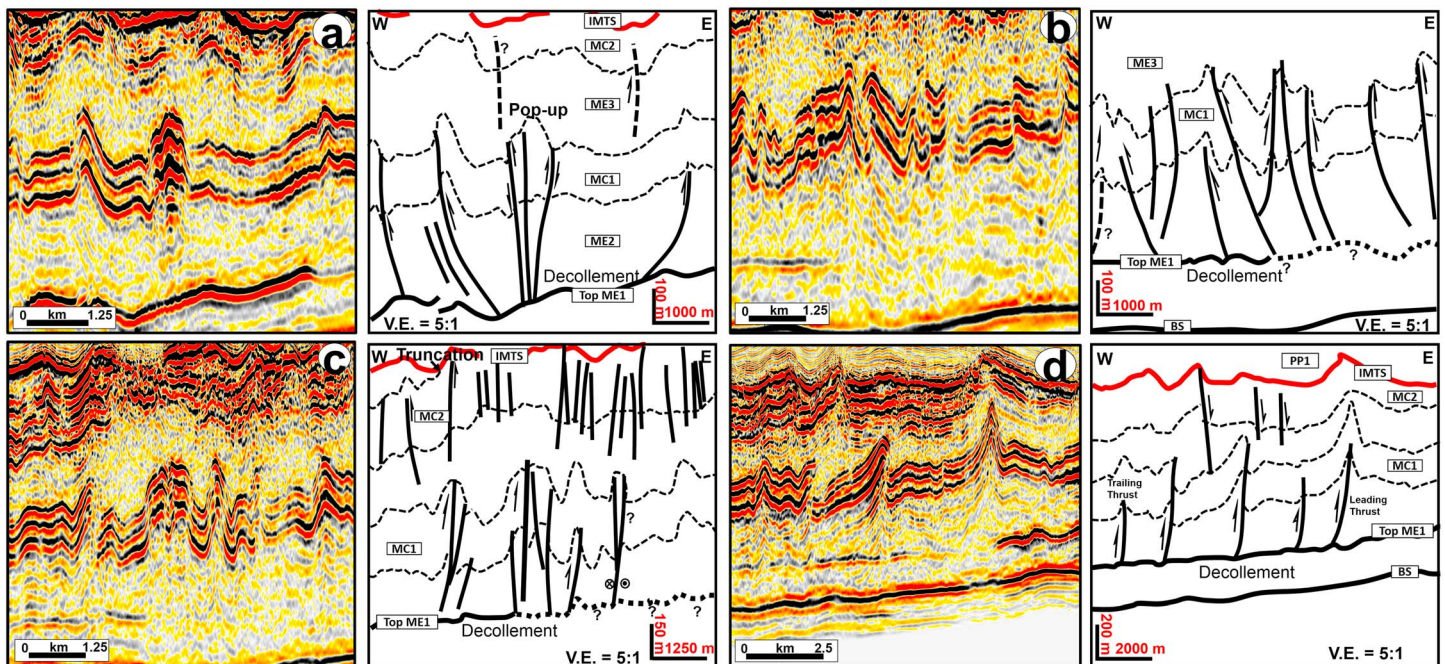


**Figure 14.** Examples of intrasalt deformation in Zone 2. Note the compressional pop-up structure in (a), intense thrust and back thrust faulting in (b), toplap relationship between the MC2 and the IMTS in (c), and a train of thrust faults in (d).

Bonora, 2001). Strike-slip faults also appear to influence the occurrence of well-developed triangular thrust zones. Where the NE-SW sinistral faults do not interact with thrusts, they appear as individual, steeply dipping to vertical faults with low throws (Figure 10e). We recognize that strike-slip faulting probably has a great influence on the contractional structures in the area, superimposing offsets and deformation zones where they interact with thrust faults and compressional folds.

The thrust faults in the study area displace the MC1, MC2, and the Plio-Quaternary succession and here we present two possible models to elucidate the observed fault geometry. In the first model, we considered the N-S intrasalt thrusts as small-scale forethrusts created by significant downslope gravity gliding to the west before the deposition of the MC2. This could have generated the forward propagation of a forethrust train in a piggyback sequence (Letouzey et al., 1995), while the NW-SE oriented thrusts, on the other hand, are probably related to the main contractional phase that occurred during the Late Pliocene (Cartwright et al., 2012) or a later Messinian deformation phase (Gvirtzman et al., 2013). In a second model, we propose that the N-S trending thrust faults are back thrusts formed after the main contractional phase that created the NW-SE trending forethrusts occurred, in a modified, clockwise rotated, contractional regime (Figure 10a). Alsop et al. (2017) shows that similar mechanisms work in fold and thrust systems in MTDs around the Dead Sea Basin, and their model could be applicable to the intrasalt sequence in the Levant Basin as well. Hence, the NW-SE oriented master faults in the case acted as buttresses and continued salt movement after the main deformation phase forced sediments into the footwall of the back thrusts producing a train of back thrusts (see Alsop et al., 2017). This would cause the hangingwall of the back thrusts to remain passive, but steepening of the thrusts eastward toward the buttress would cause some bed thickening (Alsop et al., 2017). This process would unavoidably also affect the overlying sediments and prompt the emergence of the NNW-SSE thrust faults within the MC2 and the overburden. We acknowledge that physical and numerical models indicate that strain-induced thickness changes occurs in multilayered evaporites (Allen et al., 2016), but we argue that this is not the case in this area because thickness changes are inconsistent (Figures 10a and 10b) while the transparent halite is pure and uniform (Feng et al., 2016).

Our work demonstrates the predominance of the NW-SE thrust faults within the MC1 and the occurrence of two additional thrust fault types, that is, N-S and NNW-SSE thrust faults. At lower stratigraphic intervals, the intrasalt thrust faults progress from the NW-SE trend in the MC1 to NNW-SSE trend in the MC2 and at the IMTS, respectively. This adjustment in trend is marked by a distinct decrease in the dipping of

reflections upward in the salt sequence (Figure 9) and possibly represents localized deformational events. Nonetheless, we propose three different episodes of contractional tectonics related to the formation of N-S, NW-SE, and NNW-SSE thrust faults in the study area (Figures 9 and 10b) and conclude that the NW-SE faulting in MC1 induce NW-SE to NNW-SSE trending folding in MC2 and on the IMTS reflector. Although the MC2 package and the IMTS surface are folded similarly, they are not conformably deposited. The MC2 is much more deformed by folding and faulting than the overlying erosional surface indicating that some salt deformation occurred before the intra-Messinian erosion event. The clockwise rotation of this deformational trend is suspected to be related to the contractional regime that produced the N-S trending faults in MC1, provided these N-S faults were formed after the NW-SE thrust faults.

The NNW-SSE oriented suprasalt thrust faults generally involve all layers from the MC2 to the seabed, but many of them do not offset the IMTS and are cut by the MTDs, especially in the central part of the study area. The orientation of these thrust faults in the Plio-Quaternary overburden is hard to explain in terms of gravitational gliding (Figure 1). One would intuitively expect that the salt would glide downslope toward the deep basin and form N-S to NE-SW oriented contractional structures (see Gradmann et al., 2005; Loncke et al., 2006). Based on the occurrence of extensional faults to the east, one could also argue for structures that would be subparallel to the basin margin producing N-S to NE-SW contractional faults and folds. We propose that gravitational spreading induced by Nile Cone progradation together with northward gravitational gliding in the deep basin locally forces the salt motion updip by horizontal compressional stress due to lateral expansion toward the basin margin in the study area (Fletcher et al., 1995; Hudec & Jackson, 2006, 2009). Similar thrusting toward the salt margin is seen in obsidian lava flows as well as salt glaciers in Iran (M. t. Jackson & Talbot, 1986; Waltham, 2008). Suspected roof-edge thrusts upsection from the salt sheet tip are likely to be overprinted by the dominant extensional faulting at the margin. This mechanism would explain the disarrangement of the deformation trend but raises some timing issues that will be discussed later. Cartwright et al. (2012) explained this disconnection in the shortening direction by radial gravity spreading caused by progradation of the Nile Cone. We see this as a plausible alternative explanation that might also be enforced by gravitational gliding/crustal flexure in front of the Nile Cone due to extreme loading. A third explanation is that the extensive contraction in the basin, especially the NNW-SSE thrust faults that affected the MC2 and the overburden, is related to strike-slip tectonics related to the Dead Sea Transform and the reorganization of the African-Eurasian plate boundary (Bowman, 2011; Gvirtzman et al., 2013).

The two main sets of normal faults in the study area are prominent in the extensional domain toward the basin margin (Figure 8). The first set consists of large-scaled, listric normal growth faults that are parallel to the present-day coastline. Based on their changing displacement trend, prominent above the MTDs (see Figure 10f), we hypothesize that this fault set has been reactivated consequent to NNE-SSW compression in recent times. Alternatively, they are formed as a response to basin rotation caused by reorganization of the African and Eurasian plates or the progression of the Dead Sea Transform (Roveri & Manzi, 2006; Tibor & Ben-Avraham, 2005). The second set of normal faults is generally planar and parallel to the listric master faults. Although these faults have associated grabens, the ideal horst-graben systems are rarely seen in the study area. Instead, asymmetric horst-graben systems are seen in a belt between Zone 1 and Zone 2 (Figure 8). Block rotation associated with normal faulting is also seen in this area, which is expected above a basal detachment or brittle-ductile transition (Lister et al., 1986; Wernicke & Burchfiel, 1982). Interestingly, tilted blocks without internal deformation and rollover structures are seen along the same faults, indicating a heterogeneous progression of faulting. The upper tips of the second set of normal faults are truncated at the base of the overlying MTD (see Omosanya and Alves, 2014; Eruteya et al., 2016). Hence, the second set of normal faults are late stage normal faults most likely formed prior to the deposition of the MTDs.

## 5.2. Timing of Deformation

Strike-slip faulting occurs throughout the study area, and some of the deeply rooted strike-slip faults appear to extend down to the top-ME1 reflector. Since strike-slip faults do not usually yield a large vertical displacement, they are hard to visualize within the Messinian salt sequence. It is therefore not clear if the master strike-slip faults penetrate the salt package, or if the halite intervals acted as detachment layers separating the strike-slip faults. In map view, the strike-slip faults can be seen to displace the large-scale thrust faults and related antiforms, thus indicating that the strike-slip faulting was initiated and/or continued after the

main phase of contractional deformation (see Figures 11 and 13b). However, seismic stratigraphic markers such as onlapping reflections at the tops of the large-scaled thrust faults in Quaternary strata are also seen in association with the strike-slip, suggesting that these two processes overlap in time and have influenced one another (Figures 12a and 12b, and 13a). Strike-slip movement being predominant within MC2 and overburden signify regional deformation interpreted to reflect the reorganization of the Eurasia-Africa plate boundary in Pliocene-Pleistocene (Bowman, 2011; Hall et al., 2005).

The timing of the intrasalt deformation is somewhat less obvious than in the post-Messinian strata. There is a clear connection between the observed faulting and folding of the intrasalt clastic sequences and deformation of the IMTS surface and overlying sediment. However, it appears that not all salt deformation can be traced to shallower layers. This is especially true for the N-S trending folding and faulting. As previously discussed, the small-scale structures seen in MC1 are not detectable in the overlying MC2 or on the IMTS surface (Figures 7 and 12a). We believe this reflects an earlier, less dominant, local deformation phase than the regional NW-SE trending contractional features. As the deformation is restricted to the MC1, we consider that this deformation phase represents rapid, syn-Messinian halokinesis due to local uplift along the continental margin and/or basin tilting (Bar, 2009; Buchbinder & Zilberman, 1997; Gvirtzman et al., 2013) occurring before the deposition of the MC2 sequence.

The second phase of contractional deformation is much more dominant than the low-amplitude N-S structures. The NW-SE trending folding and faulting seen in the study area is the footprint of basin-wide salt tectonics previously described by Allen et al. (2016), Cartwright et al. (2012), Gvirtzman et al. (2013), and Netzeband et al. (2006). The discontinuity of the MC2 package and its truncation of the IMTS surface throughout the study area is one of the key evidence for syn-Messinian deformation. Homogeneous deposition of salt flattens the seafloor faster than any other depositional process (Gvirtzman et al., 2013). Thus, we see it as highly probable that the seabed in the basin remained close to horizontal throughout the Messinian. To account for the truncation of the MC2 package, a significant amount of deformation influencing the MC2 must thus have occurred before the formation of the erosional unconformity, IMTS. The dominant NW-SE to NNW-SSE deformation pattern can be traced from the MC1 package to the seabed (Figures 1b, 5, and 9). Individual thrust faults cannot be traced through all these layers, probably because the transparent halite packages acted as detachment surfaces. Some of the large-scale emergent thrust faults, however, are rooted at the base of the MC2 package where the overlying ME4 sequence is not present. Hence, the N-S and NW-SE thrust faults are syn-Messinian structures. Consequently, where the suprasalt thrust faults are not cut by MTDs, footwall thickening and onlapping relationships with younger sediments below the seabed are seen, indicating that the main deformation phase occurred in the Plio-Pleistocene.

The two different types of normal faulting in Zone 1 demonstrate quite different structural geometries (Figures 4c and 4d, and 8a). The majority of the planar extensional faults that produce the horst-graben structures and fault trains do not cut the IMTS surface and have generally small throws. Some of them, however, displace the IMTS vertically on the order of several hundred meters, but it can be difficult to determine the lower detachment surface due to the transparent nature of the ME3 package. It appears that some of the bigger faults might also influence the MC1, but due to the amount of deformation in this package, it is hard to confirm if the observed faulting is coupled to the overlying normal faults or if it is a response to local deformation and/or strike-slip faulting. The amount of displacement in these fault planes seems to be quite constant from the IMTS and up to the base of the MTDs. Some of them even offset the base of the MTDs more than the major growth faults (Figures 8a and 10f) to a maximum of ~100 m. The major, listric, growth faults, however, offset the IMTS significantly more than the planar faults (Figure 10f). Based on these observations, we propose that the large-scaled growth faults near the basin margin have been active at least since the end of the Messinian. The extensional faulting observed westward of the growth faults has a fairly constant vertical throw from the IMTS almost to where they truncate the MTD package. This indicates that this normal faulting was initiated during a period of deformation in the Plio-Quaternary and was later cut by MTDs.

### 5.3. Variation in Structural Styles From Syn-Messinian to Post-Messinian Strata

Our interpretation suggests that all the transparent strata within the salt act like individual levels of decollement. The key information from the structural maps (Figure 9) and other seismic sections is that there is a general decrease in fault density from IMTS to MC1, (also reported by Allen et al., 2016; Feng et al., 2016; Gvirtzman et al., 2013). The offset and frequency of faults are also larger at the IMTS horizon than in the



deeper intrasalt packages, largely due to the extensive deformation of the Plio-Quaternary overburden, and not internal salt deformation (see Figures 6a, 8, and 10d). Only very rarely do large faults in MC1 offset the IMTS surface. Where this occurs, it is likely due to an overlapping relationship with the overlying strike-slip faults, or at large-scale normal faults (Figures 8 and 13b).

Folding in the Messinian layers slightly decreases from the IMTS to the MC2 and then increases within the MC1 (Figure 9). This observation conflicts with the results of previous studies in the area and is the key to unraveling the structural development of the study area. Folds within the topmost evaporite units are oriented in NNW-SSE direction as opposed to the NW-SE and N-S orientations of the underlying folds within the MC1 (Figure 9), suggesting that the folds were produced by ENE-WSW, NE-SW, and E-W directed compressional forces. The small-scaled N-S folding conceivably represents a short-lived and early deformation phase in the MC1 or are a result of a concentrated small-scaled Poiseuille flow similar to the model of Cartwright et al. (2012). Alternatively, these small thrusts and folds were simply overprinted by the large-scale deformation that affected the IMTS surface. We argue that the N-S thrusts are related to E-W compressional forces caused by local uplift of the Levant margin during the Messinian (see Gvirtzman et al., 2013; Bar, 2009; Buchbinder & Zilberman, 1997).

As for the dominant NW-SE oriented, NE verging thrust faults within the MC1, these are assumed to be related to a later deformation phase, which is much more dominant throughout the study area and affects both the MC1 and MC2 strata as well as the IMTS surface and overburden (Figures 7 and 10b and 10c). However, this is not a consistent relationship, as some of the major thrusts within the MC1 do not interact with the MC2 at all, which, quite to the contrary, onlap the fault-bend folds (Figure 14d). This means that the thrusting has been active since deposition of the MC1, that it has occurred in several phases, or that the ME3 layer has locally absorbed all deformation above some of the thrusts. This extensive deformation is still active, but it has not been constant throughout this time. The orientation of the thrust faults and hinge lines of the folds progresses from the NW-SE in the MC1 to NNW-SSE at the IMTS, supporting syn-Messinian deformation of the salt (Figure 9). Furthermore, the MC1 and MC2 display different patterns of local faulting throughout the study area. Figure 14d presents an example where the MC1 is heavily deformed by thrusting, whereas the overlying MC2 is subject to smaller-scale normal faulting. The MC2 is to a large degree equally displaced as the IMTS, a trend that is not consistent within the deeper MC1.

Based on the discussion above, we propose a polyphase deformation model of the Levantine Basin since the onset of the MSC. First, margin uplift during the Messinian (Steinberg et al., 2010) initiated gravity gliding of the salt toward the west, thereby producing the N-S trending, W verging, folding, and thrust faulting before deposition of MC2 package. The NW-SE oriented, NE verging deformation was initiated after the deposition of the MC2 package where thrust complexes in the MC1 strata generated folding, and occasional thrusting of the overlying sediments. This deformation continued throughout the intra-Messinian erosion event, that is, the IMTS surface, and thus account for both the truncation of the MC2 sediments and initial folding of the IMTS horizon. This folding of the MC2 package and the IMTS was later overprinted by the dominant post-Messinian deformation phase involving all sedimentary layers from the MC2 to the present-day seabed. The main deformation phase overlaps in time with the deposition of MTDs in the study area during a time of frequent slope failures initiated in the Late Pliocene (Eruteya et al., 2016). This deformation altered the deformation trend in the involved layers from NW-SE to NNW-SSE. It is possible that the last two deformation phases are related to the same driving mechanism(s) and that the initiation of basin wide post-Messinian strike-slip faulting related to the Dead Sea Transform activity has rotated the contractional forces. An alternative interpretation is that the NW-SE oriented deformation in the MC1 was driven by northward gravity gliding of the salt toward the Cyprus Arc subduction zone, whereas the later phase of deformation was driven by gravitational spreading of the Nile Cone initiated in Early Pliocene (Ben-Gai et al., 2005; Gardosh et al., 2008; Gvirtzman et al., 2013).

## 6. Conclusions

High resolution, 3-D seismic reflection data from offshore Levantine Basin, Israel, has been used to provide a detailed structural framework and evolution of a salt giant. This study has used multiple approaches that include seismic interpretation, seismic attribute analysis, and structural plots to propose a new polyphase deformation model for the intrasalt layers in the study area and, by extension, the overburden layers. We

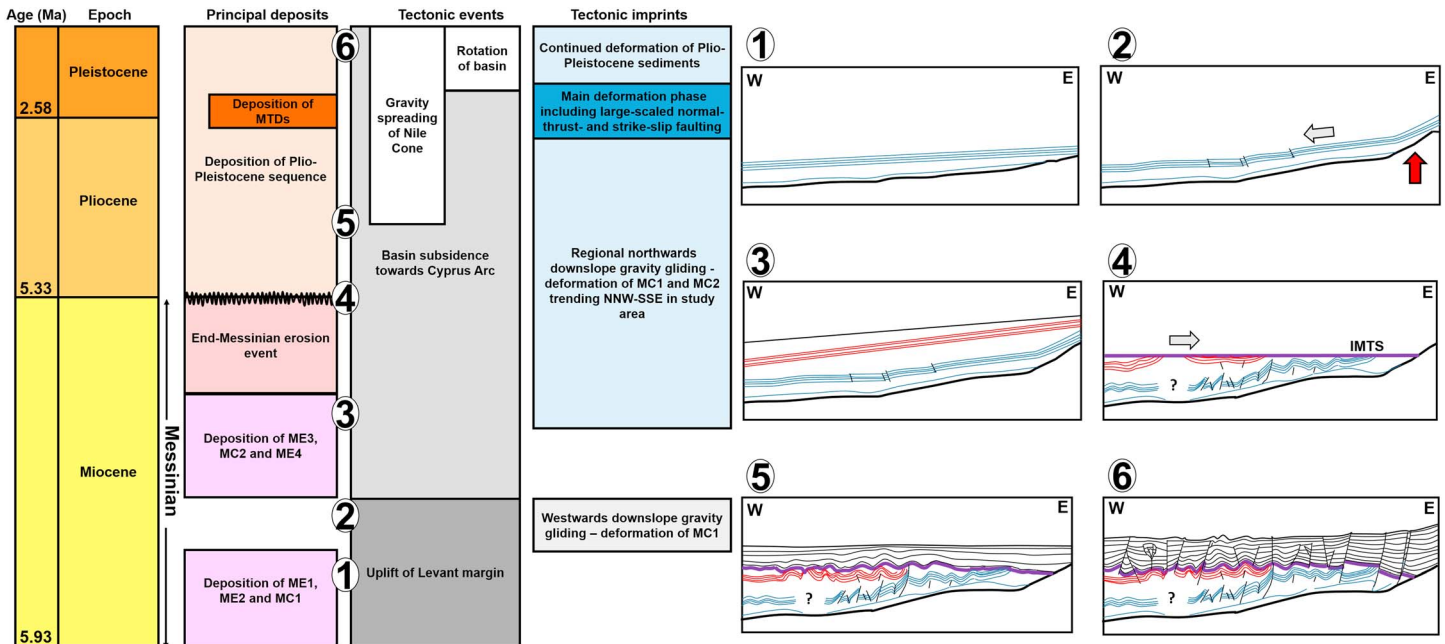


**Figure 15.** Conceptual model for the tectonic evolution of the study area.

present three distinct sets of contractional faulting affecting the Messinian salt sequence in the Levantine basin based on their orientation, geometry, and decollement level. The transparent halite strata acted as decollement layers at different stratigraphic intervals within the Messinian deposits during three phases of contractional deformation in the basin since the initiation of the MSC. Importantly, we show that the first two phases mainly involved deformation of the Messinian salt package, while the third mainly influenced the Plio-Quaternary overburden. This third deformation phase represents a time when extensional and complex salt tectonics occurs throughout the basin and remains active. In addition to large-scale thrust faults, strike-slip and normal faults occur at approximately the same time and were simultaneously triggered in response to basin rotation as a result of the reorganization of the African-Eurasian plate boundary and activity at the Dead Sea Transform or radial gravity spreading of the Nile Cone. In the study area, the intrasalt deformation is dominated by a late-Messinian syn-depositional deformation phase. Faulting occurred mainly in the MC1 sequence, forcing the overlying MC2 package to fold and be driven by gravity, gliding toward the Cyprus Arc. The first deformation phase occurred shortly after deposition of the MC1 and was caused by regional uplift along the Levant shelf. This triggered downslope salt movement to the west, producing a set of N-S trending thrust faults and folds, which were slightly overprinted by the dominant NW-SE oriented deformation. Large-scaled normal faults along the basin margin have been active since the end of the Messinian and are directly coupled to the contractional domain in the basin. An overview of the conceptual model proposed is presented in Figure 15. Our study lends weight to the report of poly-phase deformation of the intra-Messinian layers and has wider implications for regional tectonic evolution in the Levantine Basin.

#### Acknowledgments

The authors would like to acknowledge Christopher Jackson and an anonymous reviewer for their constructive reviews that improved the quality of this paper. We would also thank the Editor and Associate Editors for their effort. Kyrre is grateful to the Department of Geoscience and Petroleum, Norwegian University of Science and Technology (NTNU), for sponsoring his PhD work. Kamal hereby expresses his sincere appreciation to the European Cooperation in Science and Technology (COST) under the framework of COST Action CA15103 (MEDSALT) for funding his participation in this work via his short-term scientific mission (STSM) to the Basin Analysis and Petrophysical Laboratory, University of Haifa. Access to geophysical data was granted as part of the STSM visit. Schlumberger is thanked for provision of Petrel® for seismic interpretation. The seismic data from the study area are accessible on approval and compliance with due process from the Ministry of National Infrastructure, Energy and Water Resources, State of Israel.

#### References

- Abul Khair, H., Cooke, D., Backé, G., King, R., Hand, M., Tingay, M., & Holford, S. (2012). *Subsurface mapping of natural fracture networks; a major challenge to be solved*. South Australia: Case study from the shale intervals in the Cooper Basin.
- Al-Abry, N., & Al-Siyabi, H. (2005). Exploration history of the intrasalt carbonate stringers in the South Oman Salt Basin, International Petroleum Technology Conference. <https://doi.org/10.2523/IPTC-10407-ABSTRACT>
- Allen, H., Jackson, C. A. L., & Fraser, A. J. (2016). Gravity-driven deformation of a youthful saline giant: The interplay between gliding and spreading in the Messinian basins of the Eastern Mediterranean. *Petroleum Geoscience*, 22(4), 340–356. <https://doi.org/10.1144/petgeo2016-034>
- Allmendinger, R. W. (1998). Inverse and forward numerical modeling of trishear fault-propagation folds. *Tectonics*, 17(4), 640–656. <https://doi.org/10.1029/98TC01907>
- Alsop, G., Marco, S., Weinberger, R., & Levi, T. (2017). Upslope-verging back thrusts developed during downslope-directed slumping of mass transport deposits. *Journal of Structural Geology*, 100, 45–61. <https://doi.org/10.1016/j.jsg.2017.05.006>

- Alves, T. M., Cartwright, J., & Davies, R. J. (2009). Faulting of salt-withdrawal basins during early halokinesis: Effects on the Paleogene Rio Doce Canyon system (Espírito Santo Basin, Brazil). *AAPG Bulletin*, 93(5), 617–652. <https://doi.org/10.1306/02030908105>
- Bar, O. (2009). The shaping of the continental margin of central Israel since the late Eocene—Tectonics, morphology and stratigraphy (PhD thesis). Beer-Sheva, Israel, Ben-Gurion University of the Negev.
- Ben-Avraham, Z. (1989). Multiple opening and closing of the eastern Mediterranean and south China basins. *Tectonics*, 8(2), 351–362. <https://doi.org/10.1029/TC008i002p00351>
- Ben-Gai, Y., Ben-Avraham, Z., Buchbinder, B., & Kendall, C. G. S. C. (2005). Post-Messinian evolution of the Southeastern Levant Basin based on two-dimensional stratigraphic simulation. *Marine Geology*, 221(1–4), 359–379. <https://doi.org/10.1016/j.margeo.2005.03.003>
- Bertoni, C., & Cartwright, J. (2015). Messinian evaporites and fluid flow. *Marine and Petroleum Geology*, 66, 165–176. <https://doi.org/10.1016/j.marpetgeo.2015.02.003>
- Bertoni, C., & Cartwright, J. A. (2006). Controls on the basinwide architecture of late Miocene (Messinian) evaporites on the Levant margin (Eastern Mediterranean). *Sedimentary Geology*, 188–189, 93–114. <https://doi.org/10.1016/j.sedgeo.2006.03.019>
- Bowman, S. A. (2011). Regional seismic interpretation of the hydrocarbon prospectivity of offshore Syria. *GeoArabia*, 16, 95–124.
- Brown, A. R. (2011). *Interpretation of three-Dimensional Seismic Data*. Society of Exploration Geophysicists and American Association of Petroleum Geologists. <https://doi.org/10.1190/1.9781560802884>
- Buchbinder, B., & Zilberman, E. (1997). Sequence stratigraphy of Miocene-Pliocene carbonate-siliciclastic shelf deposits in the eastern Mediterranean margin (Israel): Effects of eustasy and tectonics. *Sedimentary Geology*, 112(1–2), 7–32. [https://doi.org/10.1016/S0037-0738\(97\)00034-1](https://doi.org/10.1016/S0037-0738(97)00034-1)
- Cartwright, J., & Huuse, M. (2005). 3D seismic technology: The geological 'Hubble'. *Basin Research*, 17(1), 1–20. <https://doi.org/10.1111/j.1365-2117.2005.00252.x>
- Cartwright, J., Jackson, M., Dooley, T., & Higgins, S. (2012). Strain partitioning in gravity-driven shortening of a thick, multilayered evaporite sequence. *Geological Society, London, Special Publications*, 363(1), 449–470. <https://doi.org/10.1144/SP363.21>
- Cartwright, J. A., & Jackson, M. P. A. (2008). Initiation of gravitational collapse of an evaporite basin margin: The Messinian saline giant, Levant Basin, eastern Mediterranean. *Bulletin of the Geological Society of America*, 120(3–4), 399–413. <https://doi.org/10.1130/B26081X.1>
- Chemia, Z., Koyi, H., & Schmeling, H. (2008). Numerical modelling of rise and fall of a dense layer in salt diapirs. *Geophysical Journal International*, 172(2), 798–816. <https://doi.org/10.1111/j.1365-246X.2007.03661.x>
- Cox, T., & Seitz, K. (2007). *Ant tracking seismic volumes for automated fault interpretation*. Calgary, Alberta, Canada: CSPG CSEG Convention.
- Druckman, Y., Buchbinder, B., Martinotti, G. M., Tov, R. S., & Aharon, P. (1995). The buried Afik Canyon (eastern Mediterranean, Israel): A case study of a Tertiary submarine canyon exposed in Late Messinian times. *Marine Geology*, 123(3–4), 167–185. [https://doi.org/10.1016/0025-3227\(94\)00127-7](https://doi.org/10.1016/0025-3227(94)00127-7)
- Erslev, E. A. (1991). Trishear fault-propagation folding. *Geology*, 19(6), 617–620. [https://doi.org/10.1130/0091-7613\(1991\)019%3C0617:TFPF%3E2.3.CO;2](https://doi.org/10.1130/0091-7613(1991)019%3C0617:TFPF%3E2.3.CO;2)
- Eruteya, O. E., Safadi, M., Waldmann, N., Makovsky, Y., & Ben-Avraham, Z. (2016). Seismic Geomorphology of the Israel Slump Complex in the Levant Basin (SE Mediterranean). In G. Lamarche, et al. (Eds.) *Submarine mass movements and their consequences. Advances in Natural and Technological Hazards Research* (Vol 41). Cham: Springer. [https://doi.org/10.1007/978-3-319-20979-1\\_4](https://doi.org/10.1007/978-3-319-20979-1_4)
- Eruteya, O. E., Waldmann, N., Schalev, D., Makovsky, Y., & Ben-Avraham, Z. (2015). Intra- to post-Messinian deep-water gas piping in the Levant Basin, SE Mediterranean. *Marine and Petroleum Geology*, 66, Part, 246–261. <https://doi.org/10.1016/j.marpetgeo.2015.03.007>
- Fang, J., Zhou, F., & Tang, Z. (2017). Discrete fracture network modelling in a naturally fractured carbonate reservoir in the Jingbei Oilfield, China. *Energies*, 10(2), 183. <https://doi.org/10.3390/en10020183>
- Feng, Y. E., & Reshef, M. (2016). The Eastern Mediterranean Messinian salt-depth imaging and velocity analysis considerations. *Petroleum Geoscience*, 22(4), 333–339. <https://doi.org/10.1144/petgeo2015-088>
- Feng, Y. E., Yankelzon, A., Steinberg, J., & Reshef, M. (2016). Lithology and characteristics of the Messinian evaporite sequence of the deep Levant Basin, eastern Mediterranean. *Marine Geology*, 376, 118–131. <https://doi.org/10.1016/j.margeo.2016.04.004>
- Fletcher, R. C., Hudec, M. R., & Watson, I. A. (1995). Salt glacier and composite sediment-salt glacier models for the emplacement and early burial of allochthonous salt sheets. In M. P. A. Jackson, D. G. Roberts, & S. Snelson (Eds.), *Salt tectonics: a global perspective, AAPG Memoir* (Vol. 65, pp. 77–108). <https://doi.org/10.1306/M65604C5>
- Frey Martinez, J., Cartwright, J., & Hall, B. (2005). 3D seismic interpretation of slump complexes: Examples from the continental margin of Israel. *Basin Research*, 17(1), 83–108. <https://doi.org/10.1111/j.1365-2117.2005.00255.x>
- Fuchs, L., Koyi, H., & Schmeling, H. (2014). Numerical modeling on progressive internal deformation in down-built diapirs. *Tectonophysics*, 632, 111–122. <https://doi.org/10.1016/j.tecto.2014.06.005>
- Gardosh M., Druckman, Y., Buchbinder, B., & Calvo, R. (2008). The Oligo-Miocene deepwater system of the Levant Basin, Geophysical Institute of Israel, rep. GII 446/426/08; geological survey of Israel, rep. GSI/33/2008, Jerusalem.
- Gardosh M., Druckman, Y., Buchbinder, B., & Rybakov, M. (2006). The Levant Basin offshore Israel: Stratigraphy, structure, tectonic evolution and implications for hydrocarbon exploration., Geological Survey of Israel, report GSI/14/2006, Jerusalem.
- Gardosh, M. A., Garfunkel, Z., Druckman, Y., & Buchbinder, B. (2010). Tethyan rifting in the Levant Region and its role in Early Mesozoic crustal evolution. *Geological Society, London, Special Publications*, 341(1), 9–36. <https://doi.org/10.1144/SP341.2>
- Garfunkel, Z. (1998). Constrains on the origin and history of the Eastern Mediterranean basin. *Tectonophysics*, 298(1–3), 5–35. [https://doi.org/10.1016/S0040-1951\(98\)00176-0](https://doi.org/10.1016/S0040-1951(98)00176-0)
- Geluk, M. (1998). Internal tectonics of salt structures. *Journal of Seismic Exploration*, 7, 237–250.
- Gorini, C., Montadert, L., & Rabineau, M. (2015). New imaging of the salinity crisis: Dual Messinian lowstand megasequences recorded in the deep basin of both the eastern and western Mediterranean. *Marine and Petroleum Geology*, 66, 278–294. <https://doi.org/10.1016/j.marpetgeo.2015.01.009>
- Gradmann, S., Hübscher, C., Ben-Avraham, Z., Gajewski, D., & Netzeband, G. (2005). Salt tectonics off northern Israel. *Marine and Petroleum Geology*, 22(5), 597–611. <https://doi.org/10.1016/j.marpetgeo.2005.02.001>
- Gvirtzman, Z., Manzi, V., Calvo, R., Gavrieli, I., Gennari, R., Lugli, S., et al. (2017). Intra-Messinian truncation surface in the Levant Basin explained by subaqueous dissolution. *Geology*, 45(10), 915–918. <https://doi.org/10.1130/G39113.1>
- Gvirtzman, Z., Reshef, M., Buch-Leviatan, O., & Ben-Avraham, Z. (2013). Intense salt deformation in the Levant Basin in the middle of the Messinian Salinity Crisis. *Earth and Planetary Science Letters*, 379, 108–119. <https://doi.org/10.1016/j.epsl.2013.07.018>
- Gvirtzman, Z., Reshef, M., Buch-Leviatan, O., Groves-Gidney, G., Karcz, Z., Makovsky, Y., & Ben-Avraham, Z. (2015). Bathymetry of the Levant basin: Interaction of salt-tectonics and surficial mass movements. *Marine Geology*, 360, 25–39. <https://doi.org/10.1016/j.margeo.2014.12.001>



- Hall, J., Calon, T., Aksu, A., & Meade, S. (2005). Structural evolution of the Latakia Ridge and Cyprus Basin at the front of the Cyprus Arc, eastern Mediterranean Sea. *Marine Geology*, 221(1-4), 261–297. <https://doi.org/10.1016/j.margeo.2005.03.007>
- Hardy, C., Homberg, C., Eyal, Y., Barrier, É., & Müller, C. (2010). Tectonic evolution of the southern Levant margin since Mesozoic. *Tectonophysics*, 494(3-4), 211–225. <https://doi.org/10.1016/j.tecto.2010.09.007>
- Hsü, K. J., Ryan, W. B. F., & Cita, M. B. (1973). Late Miocene desiccation of the Mediterranean. *Nature*, 242(5395), 240–244.
- Hübscher, C., Betzler, C., & Reiche, S. (2016). Seismo-stratigraphic evidences for deep base level control on middle to late Pleistocene drift evolution and mass wasting along southern Levant continental slope (Eastern Mediterranean). *Marine and Petroleum Geology*, 77, 526–534. <https://doi.org/10.1016/j.marpetgeo.2016.07.008>
- Hübscher, C., Cartwright, J., Cypionka, H., De Lange, G., Robertson, A., Suc, J.-P., & Urai, J. (2007). Global look at salt giants. *Eos*, 88(16), 177–179. <https://doi.org/10.1029/2007EO160002>
- Hudec, M. R., & Jackson, M. P. (2006). Advance of allochthonous salt sheets in passive margins and orogens. *AAPG Bulletin*, 90(10), 1535–1564. <https://doi.org/10.1306/05080605143>
- Hudec, M. R., & Jackson, M. P. (2007). Terra infirma: Understanding salt tectonics. *Earth-Science Reviews*, 82(1-2), 1–28. <https://doi.org/10.1016/j.earscirev.2007.01.001>
- Hudec, M. R., & Jackson, M. P. (2009). Interaction between spreading salt canopies and their peripheral thrust systems. *Journal of Structural Geology*, 31(10), 1114–1129. <https://doi.org/10.1016/j.jsg.2009.06.005>
- Jackson, C. A., Jackson, M. P., Hudec, M. R., & Rodriguez, C. (2014). Internal structure, kinematics, and growth of a salt wall: Insights from 3-D seismic data. *Geology*, 42(4), 307–310. <https://doi.org/10.1130/G34865.1>
- Jackson, C. A.-L., Jackson, M. P., Hudec, M. R., & Rodriguez, C. R. (2015). Enigmatic structures within salt walls of the Santos Basin—Part 1: Geometry and kinematics from 3D seismic reflection and well data. *Journal of Structural Geology*, 75, 135–162. <https://doi.org/10.1016/j.jsg.2015.01.010>
- Jackson, M., Cornelius, R., Craig, C., Gansser, A., Stöcklin, J., & Talbot, C. (1990). Salt diapirs of the Great Kavir, central Iran. *Geological Society of America Memoirs*, 177, 1–150. <https://doi.org/10.1130/MEM177-p1>
- Jackson, M. t., & Talbot, C. (1986). External shapes, strain rates, and dynamics of salt structures. *Geological Society of America Bulletin*, 97(3), 305–323. [https://doi.org/10.1130/0016-7606\(1986\)97%3C305:ESSRAD%3E2.0.CO;2](https://doi.org/10.1130/0016-7606(1986)97%3C305:ESSRAD%3E2.0.CO;2)
- Johansen, S. E. (2013). Composition of seismic facies: A case study. *AAPG Bulletin*, 97(10), 1645–1656. <https://doi.org/10.1306/03271312119>
- Johansen, S. E., Kibsgaard, S., Andresen, A., Henningsen, T., & Granli, J. R. (1994). Seismic modeling of a strongly emergent thrust front, West Spitsbergen fold belt, Svalbard. *AAPG Bulletin*, 78, 1018–1027.
- Jones, I. F., & Davison, I. (2014). Seismic imaging in and around salt bodies. *Interpretation*, 2(4), SL1–SL20. <https://doi.org/10.1190/INT-2014-0033.1>
- Katz, O., Reuven, E., & Aharonov, E. (2015). Submarine landslides and fault scarps along the eastern Mediterranean Israeli continental-slope. *Marine Geology*, 369, 100–115. <https://doi.org/10.1016/j.margeo.2015.08.006>
- Lazar, M., Lang, G., & Schattner, U. (2016). Coincidence or not? Interconnected gas/fluid migration and ocean—Atmosphere oscillations in the Levant Basin. *Geo-Marine Letters*, 36(4), 293–306. <https://doi.org/10.1007/s00367-016-0447-5>
- Letouzey, J., Colletta, B., Vially, R., & Chermette, J. (1995). Evolution of salt-related structures in compressional settings. In M. P. A. Jackson, D. G. Roberts, & S. Snelson (Eds.), *Salt tectonics: a global perspective*, AAPG Memoir (Vol. 65, pp. 41–60).
- Lisle, R. J. (1994). Detection of zones of abnormal strains in structures using Gaussian curvature analysis. *AAPG Bulletin*, 78, 1811–1819.
- Lister, G., Etheridge, M., & Symonds, P. (1986). Detachment faulting and the evolution of passive continental margins. *Geology*, 14(3), 246–250. [https://doi.org/10.1130/0091-7613\(1986\)14%3C246:DFATEO%3E2.0.CO;2](https://doi.org/10.1130/0091-7613(1986)14%3C246:DFATEO%3E2.0.CO;2)
- Loncke, L., Gaullier, V., Mascle, J., Vendeville, B., & Camera, L. (2006). The Nile deep-sea fan: An example of interacting sedimentation, salt tectonics, and inherited subsalt paleotopographic features. *Marine and Petroleum Geology*, 23(3), 297–315. <https://doi.org/10.1016/j.marpetgeo.2006.01.001>
- McClay, K., & Bonora, M. (2001). Analog models of restraining stepovers in strike-slip fault systems. *AAPG Bulletin*, 85, 233–260.
- Netzeband, G., Hübscher, C., & Gajewski, D. (2006). The structural evolution of the Messinian evaporites in the Levantine Basin. *Marine Geology*, 230(3-4), 249–273. <https://doi.org/10.1016/j.margeo.2006.05.004>
- Omosanya, K. O., & Alves, T. M. (2014). Mass-transport deposits controlling fault propagation, reactivation and structural decoupling on continental margins (Espírito Santo Basin, SE Brazil). *Tectonophysics*, 628, 158–171. <https://doi.org/10.1016/j.tecto.2014.04.045>
- Peters, J., Filbrandt, J., Grotzinger, J., Newall, M., Shuster, M., & Al-Siyabi, H. (2003). Surface-piercing salt domes of interior North Oman, and their significance of the Ara carbonate “stinger” hydrocarbon play. *GEOARABIA-MANAMA*, 8, 231–270.
- Raith, A., Strozyk, F., Visser, J., & Urai, J. (2016). Evolution of rheologically heterogeneous salt structures: A case study from the NE Netherlands. *Solid Earth*, 7(1), 67–82. <https://doi.org/10.5194/se-7-67-2016>
- Rank-Friend, M., & Elders, C. F. (2004). The evolution and growth of central graben salt structures, Salt Dome Province, Danish North Sea. *Geological Society, London, Memoirs*, 29(1), 149–164. <https://doi.org/10.1144/GSL.MEM.2004.029.01.15>
- Reuning, L., Schoenherr, J., Heimann, A., Urai, J. L., Littke, R., Kukla, P. A., & Rawahi, Z. (2009). Constraints on the diagenesis, stratigraphy and internal dynamics of the surface-piercing salt domes in the Ghaba Salt Basin (Oman): A comparison to the Ara Group in the South Oman Salt Basin. *GeoArabia*, 14, 83–120.
- Roveri, M., Flecker, R., Krijgsman, W., Lofi, J., Lugli, S., Manzi, V., et al. (2014). The Messinian salinity crisis: Past and future of a great challenge for marine sciences. *Marine Geology*, 352, 25–58. <https://doi.org/10.1016/j.margeo.2014.02.002>
- Roveri, M., & Manzi, V. (2006). The Messinian salinity crisis: Looking for a new paradigm? *Palaeogeography Palaeoclimatology Palaeoecology*, 238(1-4), 386–398. <https://doi.org/10.1016/j.palaeo.2006.03.036>
- Rowan, M. G. (1993). A systematic technique for the sequential restoration of salt structures. *Tectonophysics*, 228(3-4), 331–348. [https://doi.org/10.1016/0040-1951\(93\)90347-M](https://doi.org/10.1016/0040-1951(93)90347-M)
- Rowan, M. G., Peel, F. J., Vendeville, B. C., & Gaullier, V. (2012). Salt tectonics at passive margins: Geology versus models—Discussion. *Marine and Petroleum Geology*, 37(1), 184–194. <https://doi.org/10.1016/j.marpetgeo.2012.04.007>
- Ryan, W. B. (1978). Messinian badlands on the southeastern margin of the Mediterranean Sea. *Marine Geology*, 27(3-4), 349–363. [https://doi.org/10.1016/0025-3227\(78\)90039-7](https://doi.org/10.1016/0025-3227(78)90039-7)
- Sagy, Y. (2015). *Tectono-sedimentary processes in the deep Levant Basin*. Jerusalem: Geological Survey of Israel.
- Schlöder, Z., Urai, J. L., Nollet, S., & Hilgers, C. (2008). Solution-precipitation creep and fluid flow in halite: A case study of Zechstein (Z1) rock salt from Neuhof salt mine (Germany). *International Journal of Earth Sciences*, 97(5), 1045–1056. <https://doi.org/10.1007/s00531-007-0275-y>
- Schultz-Ela, D., & Walsh, P. (2002). Modeling of grabens extending above evaporites in Canyonlands National Park, Utah. *Journal of Structural Geology*, 24(2), 247–275. [https://doi.org/10.1016/S0191-8141\(01\)00066-9](https://doi.org/10.1016/S0191-8141(01)00066-9)

- Shahar, J. (1994). The Syrian arc system: An overview. *Palaeogeography Palaeoclimatology Palaeoecology*, *112*(1-2), 125–142. [https://doi.org/10.1016/0031-0182\(94\)90137-6](https://doi.org/10.1016/0031-0182(94)90137-6)
- Steinberg, J., Gvirtzman, Z., & Folkman, Y. (2010). New age constraints on the evolution of the Mt Carmel structure and its implications on a Late Miocene extensional phase of the Levant continental margin. *Journal of the Geological Society*, *167*(1), 203–216. <https://doi.org/10.1144/0016-76492009-089>
- Strozyk, F., Urai, J. L., van Gent, H., de Keijzer, M., & Kukla, P. A. (2014). The internal structure of salt: Insights from a regional 3D seismic study of the Permian Zechstein 3 intra-salt stringer in the Northern Netherlands, and its implications for salt tectonics, EGU General Assembly Conference Abstracts (p. 5708).
- Strozyk, F., Van Gent, H., Urai, J., & Kukla, P. A. (2012). 3D seismic study of complex intra-salt deformation: An example from the Upper Permian Zechstein 3 stringer, western Dutch offshore. *Geological Society, London, Special Publications*, *363*(1), 489–501. <https://doi.org/10.1144/SP363.23>
- Talbot, C., & Jackson, M. (1987). Internal kinematics of salt diapirs. *AAPG Bulletin*, *71*, 1068–1093.
- Tibor, G., & Ben-Avraham, Z. (2005). Late Tertiary paleodepth reconstruction of the Levant margin off Israel. *Marine Geology*, *221*(1-4), 331–347. <https://doi.org/10.1016/j.margeo.2005.03.005>
- Tibor, G., Ben-Avraham, Z., Steckler, M., & Fligelman, H. (1992). Late Tertiary subsidence history of the Southern Levant Margin, Eastern Mediterranean Sea, and its implications to the understanding of the Messinian event. *Journal of Geophysical Research*, *97*(B12), 17,593–17,614. <https://doi.org/10.1029/92JB00978>
- Trudgill, B. D., & Rowan, M. G. (2004). Integrating 3D seismic data with structural restorations to elucidate the evolution of a stepped counter-regional salt system, Eastern Louisiana Shelf, Northern Gulf of Mexico. *Geological Society, London, Memoirs*, *29*(1), 165–176. <https://doi.org/10.1144/GSL.MEM.2004.029.01.16>
- Van Gent, H., Back, S., Urai, J. L., & Kukla, P. (2010). Small-scale faulting in the Upper Cretaceous of the Groningen block (the Netherlands): 3D seismic interpretation, fault plane analysis and regional paleostress. *Journal of Structural Geology*, *32*(4), 537–553. <https://doi.org/10.1016/j.jsg.2010.03.003>
- Vendeville, B., & Jackson, M. (1992). The fall of diapirs during thin-skinned extension. *Marine and Petroleum Geology*, *9*(4), 354–371. [https://doi.org/10.1016/0264-8172\(92\)90048-J](https://doi.org/10.1016/0264-8172(92)90048-J)
- Vendeville, B. C. (2005). Salt tectonics driven by sediment progradation: Part I—Mechanics and kinematics. *AAPG Bulletin*, *89*(8), 1071–1079. <https://doi.org/10.1306/03310503063>
- Waltham, T. (2008). Salt terrains of Iran. *Geology Today*, *24*(5), 188–194. <https://doi.org/10.1111/j.1365-2451.2008.00686.x>
- Wernicke, B., & Burchfiel, B. (1982). Modes of extensional tectonics. *Journal of Structural Geology*, *4*(2), 105–115. [https://doi.org/10.1016/0191-8141\(82\)90021-9](https://doi.org/10.1016/0191-8141(82)90021-9)